The Ins and Outs of Melanopsin Signaling

by

Krystal R. Harrison

A dissertation submitted in partial fulfillment
of the requirements for the degree of
Doctor of Philosophy
(Molecular, Cellular and Developmental Biology)
in the University of Michigan
2020

Doctoral Committee:

Professor Kwoon Y. Wong, Chair
Professor Sara Aton
Professor Richard Hume
Professor Shawn Xu

Krystal R. Harrison

krharr@umich.edu

ORCID iD: 0000-0001-8767-5104

Dedication

To my grandfathers, William Harrison (1915 – 2014) and Ronald Long (1943-), thank you for encouraging me to pursue a doctoral degree. Although your education never exceeded the 3rd grade and high school respectively, you understood the value of obtaining a degree. Your love, wisdom, and spirit has uplifted me throughout this journey.

To the next generation of Black scientists, may my graduate school experience exhibit to you that you can achieve anything you set your mind to and with perseverance you will reap what you sow.

Acknowledgements

I am thankful to Dr. Kwoon Wong for his guidance, mentorship, and support. My first interaction with Kwoon was during my second year while I was searching to find a permanent lab. Not only did you take me in, but from day one you've invested in my matriculation as a young scientist. I joined your lab with no prior experience in neurobiology and yet you accepted me, took time to teach important concepts, reviewed literature with me and prepared me for a successful prelim. Thank you for pushing and challenging me to always dig deeper, and for giving me the encouragement needed to pursue my ideas and career goals; I could not have done this without you!

I would also like to thank the members of my thesis committee- Dr. Rich Hume, Dr. Sara Aton and Dr. Shawn Xu. You all have provided me with sound advice, feedback, and encouragement throughout the completion of this thesis. For that, I am eternally grateful.

Next, I want to thank all members of the Wong lab who've helped me along the way: Dr. Andrew Chervenak, Dr. Aaron Reifler, Dr. Xiwu Zhao, Austra Liepa, and my undergraduate mentee Sarah Resnick. Kwoon, Andrew and Aaron, thank you for genotyping the mouse lines necessary for this thesis. I know how difficult it was at times, so I appreciate your persistent efforts. To Andrew, Xiwu and Kwoon thank you for dissecting retinas prior to my intracellular injections and to Sarah thank you for working under my direction, keeping me company while

we injected in the dark, and for being a great mentee. To Austra, Andrew and Kwoon, I appreciate your devotion to maintaining mouse lines. I want to further thank Andrew and Aaron, for you both kept me sane especially when my results left me puzzled and without you, I would not have gained the encouragement to keep persevering. Andrew-you taught me valuable techniques such as intracellular injections, immunostaining, and most importantly, you served as a valuable friend and mentor. It was a pleasure working with all of you.

To professors and staff members at Kellogg Eye Center-Dr. Bret Hughes, thank you for always checking on me, giving me feedback and for being a great support system. You have been a valuable person to have in my corner throughout this journey. Dr. Cheng-mao Lin and Sarah Sheskey, members of the Functional Assessment Module, thank you for working with me and teaching me how to use the OptoMotry apparatus. Dr. David Antonetti- words can't express the gratitude I have towards you and members of your lab. In 2012, I interned with you during the summer and it was through that experience that solidified me to pursue a PhD. You knew I had the dedication needed to obtain this degree while I was still in college and for that, thank you.

To all students, faculty and staff of the Molecular, Cellular and Developmental Biology (MCDB) program, thank you. I want to say a special thank you to Mary Carr for serving as my "department mother". You always had a warm hug and smile for me whenever I would come by your office. Thank you for advocating for me when I needed it the most. To Dr. Matt Chapman, thank you for persuading me to attend U of M and to join the MCDB department. I would also

like to thank Gregg Sobocinski, the Director of MCDB's Microscope Imaging Suite who has helped me configure and set up various parameters needed for confocal imaging.

I am grateful for my funding sources throughout graduate school: the NIH, Rackham Merit Fellow, Rackham Dissertation Fellowship, and MCDB.

Last but not least, I want to thank my family and friends for their support, love, and sound advice. Thank you for keeping me encouraged throughout every step of this journey and for understanding when I couldn't attend family and social events. To my parents, THANK YOU for cultivating my love for science at an early age. From signing me up to attend science camps to driving me 10+ hours for my summer internships, you both have been my rock and without your unwavering love, I would not have made it this far. To my boyfriend, I am incredibly lucky to have the most loving partner that anyone could pray for-thank you for never letting me give up, thank you for wiping every tear I've cried and most importantly thank you for celebrating every milestone I've accomplished. When I was lonely, thank you for gifting me with a forever companion, our dog Eden.

Table of Contents

List of Figures

List of Tables

List of Chemical Solutions

Ames' Medium (Sigma Aldrich)	Normal Donkey Serum (Sigma Aldrich)
Sodium Bicarbonate (Sigma Life Science)	Lucifer Yellow (Electron Microscopy Sciences)
D-glucose (Fisher Scientific)	anti-RBPMS (Phosphosolutions)
Cesium Chloride (Sigma Aldrich)	anti-cfos (ABCAM; Santa Cruz Biotechnology)
4% Neurobiotin (Vector Laboratories)	anti-Connexin36 (Thermofisher)
Streptavidin 568 (Invitrogen, Thermofisher Scientific)	anti-Connexin45 (Thermofisher)
Phosphate Buffer Saline (Sigma Aldrich)	1M Potassium Chloride (Sigma Aldrich)
Triton X-100 (Sigma Aldrich)	16% Paraformaldehyde (Sigma Aldrich)

Abstract

Intrinsically photosensitive retinal ganglion cells (ipRGCs) are responsible for non-image-forming functions such as circadian photoentrainment, pupillary light reflex and the suppression of melatonin. Additionally, their axons innervate two main image-forming visual nuclei: the superior colliculus (SC) and the lateral geniculate nucleus (LGN). Furthermore, electrophysiology data discovered that ipRGCs signal to dopaminergic amacrine cells via AMPA/kainate glutamate receptors and to displaced amacrine cells (ACs) located in the ganglion cell layer of the retina through gap junctions. Retinal ganglion cells had never been found to signal intraretinally prior to this finding.

Several labs have been exploring how ipRGCs mediate or modulate image-forming vision through their central projections and signaling to dopaminergic ACs. However, little is known about the functional roles of gap-junction signaling from ipRGCs to displaced ACs and how ipRGCs work in conjunction with rod and cone photoreceptors to mediate image-forming visual responses. Neurobiotin tracer injections, immunostaining, and optokinetic visual behavior techniques were used in this thesis to fill in this knowledge gap. Four specific aims were accomplished: 1) understand how ipRGC-coupled ACs are distributed across the retina and identify ACs gap-junction coupled to ipRGCs, 2) test the hypothesis that connexin36 (Cx36) couples ipRGCs to displaced ACs, 3) examine the effect of glutamatergic input on ipRGC-AC coupling, and 4) assess the effect of rods, cones and melanopsin on image-forming behavior.

We found that all six ipRGC types are electrically coupled to amacrine cells, primarily via Cx36 and a few ipRGC-coupled amacrine cells are immunopositive for brain nitric oxide synthase (bNOS), neuronal nitric oxide synthase (nNOS), neuropeptide Y (NPY) or serotonin (5-HT). Additionally, we uncovered that ipRGC-AC coupling is enhanced in the presence of NMDA receptor expression in ipRGCs. Finally, we've shown that the distribution of ipRGC-coupled amacrine cells is region specific and rods, cones and melanopsin contribute to image-forming vision differently. Because ipRGCs remain light-sensitive in many blind patients suffering from rod and cone degeneration, a better understanding of the signaling by ipRGCs could lead to novel strategies to restore sight in such patients.

Chapter 1 – Introduction

1.1 The Visual System

The visual system allows us to image the world around us and without it, we would be unable to receive and process photic information in our environment. It's the most extensively studied of all senses. Images are formed in the retina by bending light rays, a process known as refraction. These light rays enter the eye through the cornea, refract, then travel through the pupil until they reach the retina, located in the back of the eye (Figure 1.1). Vision begins in the retina where photoreceptors cells convert light into electrical signals which are ultimately processed by retinal interneurons and sent to the brain to further process images in our surroundings.

1.2 Model Organism: Why Mice

A commonly used organism to study structure, function, development, and disease within the visual system is the mouse. The genetic, physiological, and behavioral characteristics of mice resemble those of humans and thus, many symptoms of human conditions can be replicated using mice. In fact, according to the National Human Genome Research Institute, mice and humans share roughly 85% of protein-coding regions and these regions are evolutionarily conserved. Using mice to understand various aspects of the visual system has allowed a variety

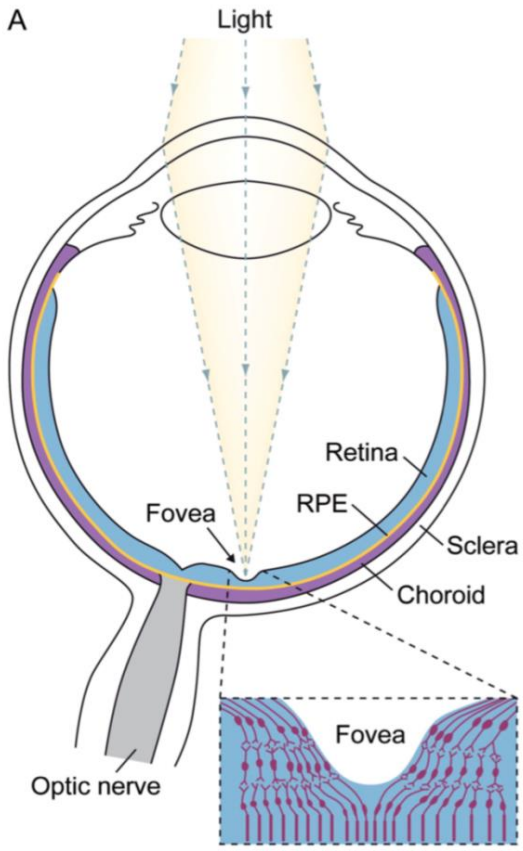

Figure 1.1: A diagram of the eye representing the visual sense organ. The retina is located towards the back of the eye (Sung and Chuang, 2010).

of genetic tool analyses to be made regarding gene function and has aided in expanding the knowledge regarding neural circuitry and the cell types responsible for retinal development. Secondly, many light-based studies can be tightly controlled *in vitro* or *in vivo* which allows researchers to address questions regarding sensory information processing in the retina. Finally, genetic manipulation of neuronal activity can be performed *in vivo*, which is simpler and more ethically acceptable than using humans. All in all, using mice provides an effective way to address and answer various questions impacting human health.

1.3 Organizational View of the Retinal Circuit

Neuronal connections within the retina allow us to transmit information in our visual scene and understand features within that space (e.g. color and direction of motion). Although the retina forms a sheet of tissue only ~200μm thick, it is comprised of five classes of neurons: rod and cone photoreceptor cells, bipolar cells, horizontal cells, amacrine cells, and ganglion cells (Figure 1.2). Photoreceptors serve as the input neurons of the retina because they are responsible for detecting photons (light) from the outside environment and converting them into electrical signals that interneurons (i.e. bipolar, horizontal, and amacrine cells) in the retina can analyze. Finally, ganglion cells are the last class of retinal neurons to receive the light-evoked signals and their axons propagate these signals along the optic nerve to provide the rest of the visual system with the necessary information for interpreting the visual scene. While there are only five classes of neurons in the retina there are many types of neurons within each class, leading to a relatively complex retinal circuit. It is estimated that the mouse retina has over 100 neuronal cell types (Masland, 2012). A schematic displaying the morphological diversity among retinal types is

shown in Figure 1.3 (Masland, 2001). Typically, neurons are divided into types based on the following characteristics: morphology, molecular contents and/or physiologic properties. Photoreceptors are unique in the sense that they contain mechanisms to initiate phototransduction- the process in which photons are converted into electrical signals. Light reaches photoreceptors located in the outer part of the retina, the region furthest from incoming light, and is absorbed by photopigment molecules. Cones and rods are two types of photoreceptors located in the outer nuclear layer of the retina. Cones are responsible for mediating vision in bright light as well as color vision (Dowling, 1965; Cohen, 1970). Cones can adapt to all backgrounds of light and are less light-sensitive than rods (Dowling, 2012). Most mammals (e.g. mice) have two cone pigment types whereas humans have three different cone populations sensitive to red, green and blue light. In contrast, there is only one kind of rod photoreceptor, yet they outnumber cone photoreceptors by ~20 fold in both mice and humans and have been extensively studied in comparison to cones (Sung and Chuang, 2010). Rods are quickly saturated by bright light and therefore, are functional mainly in dim lighting conditions (Dowling, 2012).

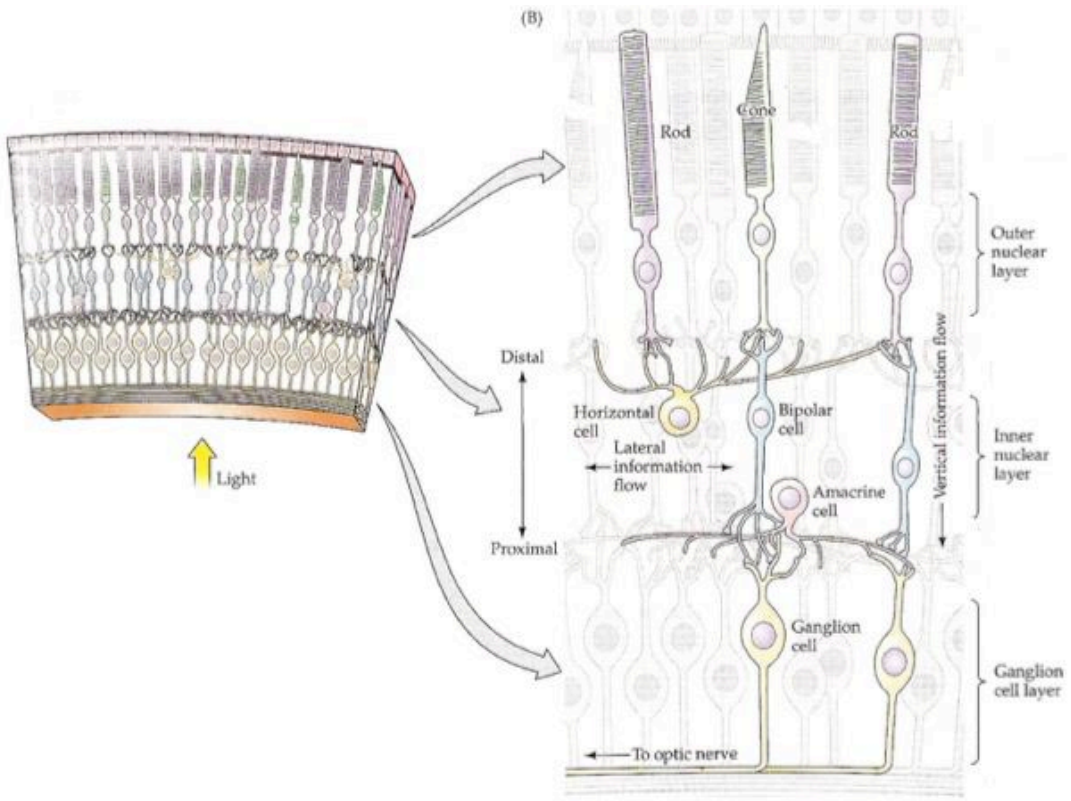

Figure 1.2: A schematic diagram of the organization of retinal neurons (Purves *et al. 2012).*

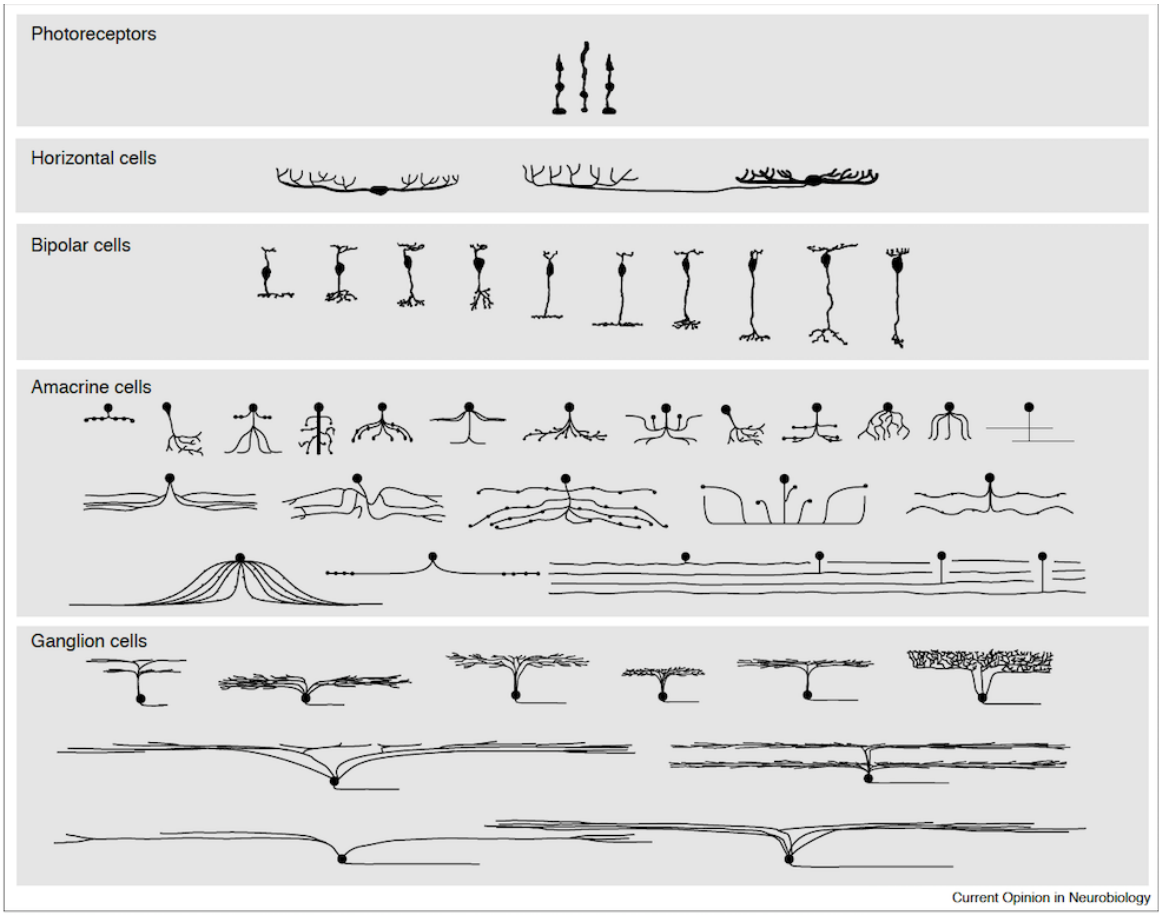

Figure 1.3: A schematic diagram of the major neuronal populations within the mammalian retina (Masland, 2001).

A majority of mammals have two types of horizontal cells, which are interconnecting neurons organized laterally. Each horizontal cell integrates input from many photoreceptors ultimately carrying out a step of signal conditioning through its ability to provide inhibitory feedback the photoreceptors, a circuit commonly known as “lateral inhibition” (Masland, 2012). Bipolar cells located in the inner nuclear layer play an important role where any signal from photoreceptors must pass through them to eventually reach ganglion cells. There are two varieties of bipolar cells: ON and OFF, which are excited by increments and decrements in light intensity respectively.

The complexity of both ACs and ganglion cells has far exceeded what was imagined at the turn of the 21st century. For every type of ganglion cell, it has been estimated that there are roughly 3 types of ACs (Masland, 2012). ACs can be defined into wide field, medium field and narrow field categories and often communicate among several strata of the inner plexiform layer which is known as “vertical inhibition.” While ACs do contain neuromodulators that act on relatively slow time scales, the majority of ACs release inhibitory neurotransmitters, GABA or glycine. These neurotransmitters and neuromodulators have been shown to modulate the light-evoked responses of retinal neurons. Little is known about many types of ACs. Some types however are fairly well known such as the AII amacrine cell which is involved in the rod pathway, the dopaminergic amacrine cell which is important for adaptation in light and dark conditions and the starburst amacrine cell which is crucial for regulating direction selectivity (Masland, 2001 a,b).

Depending on the species, there are 20-40 types of ganglion cells and each type responds differently to light and therefore, interprets distinct information from the stimulus. Retinal ganglion cells use their diverse light response to analyze four major aspects in the visual world: spatial analysis (shape), wavelength (color), direction (motion) and irradiance (light intensity). Identifying ganglion cells in the mouse retina led to several complications because ganglion cells were less distinctive in the mouse than the rabbit or monkey (O'Brien et al., 2002; Dacey, 2004).

1.4 Discovery of Intrinsically Photosensitive Retinal Ganglion Cells

For over a century, scientists believed that the retina only contains two types of photoreceptors, namely rods and cones, and that they mediate all non-image-forming (NIF) photoresponses as well as image-forming (IF) vision. However, research conducted in the past twenty years has shown that the retina contains an additional cell type responsible for NIF physiological responses to light. Studies have shown that in the absence of rod and cones, the retina was able to drive NIF functions such as pupillary light reflex (Lucas et al., 2001), the suppression of melatonin secretion (Czeisler et al., 1995), and circadian photoentrainment (Freedman et al., 1999). The experiments above led researchers in the field to hypothesize that the retina contains an additional photoreceptor responsible for mediating NIF functions in response to light.

Berson et al. sought to further identify this mysterious photoreceptor and believed that since these cells could regulate circadian photoentrainment, their axons should project to the site of the circadian pacemaker, the suprachiasmatic nucleus (SCN). After injecting a fluorescent dye into the SCN of rats to retrogradely label the cells innervating the SCN, Berson et al. found that a

small percentage (1-2%) of ganglion cells were labeled (Figure 1.4). Whole-cell recordings established that these ganglion cells respond to light directly and Berson called them intrinsically photosensitive retinal ganglion cells (ipRGCs) (Berson et al., 2002). Hatter et al. later discovered that ipRGCs contain a putative photopigment called melanopsin (Figure 1.5). Another unique feature of ipRGCs compared to rods and cones is that they depolarize in response to light and provide long-term irradiance coding (Berson et al., 2002; Wong et al., 2007).

Currently, there are six known morphologically- distinct types of ipRGCs (Figure 1.6) in mice termed M1 through M6, and five identified types in rat species termed M1 through M5 (Schmidt et al., 2008; Berson et al., 2010; Ecker et al., 2010; Schmidt et al., 2014; Reifler et al., 2015; Quattrochi et al., 2019). The dendrites of ipRGCs can ramify in the ON-sublamina and/or OFF-sublamina of the inner plexiform layer. M1 was the first ipRGC characterized and has dendrites that stratify in the OFF sublamina. The dendrites of M2 cells stratify into the ON-sublamina while the dendrites of M3 cells stratify in the ON and OFF sublaminae. Type M4 has dendrites that are dense and stratify in the ON-sublamina. M5 RGCs' dendrites stratify in the ON-sublamina and have a bushier appearance (Schmidt et al., 2008; Berson et al., 2010; Ecker et al., 2010; Schmidt et al., 2014; Reifler et al., 2015). The newly identified type, M6 has dendrites that stratify in the ON and OFF sublaminae similar to M3; however, they have relatively small receptive fields compared to M3 RGCs. In addition, each type generates different melanopsin based light responses, suggesting that these photoreceptors are functionally diverse (Figure 1.6, bottom) (Zhao et al., 2014; Walch et al., 2015; Quattrochi et al., 2019).

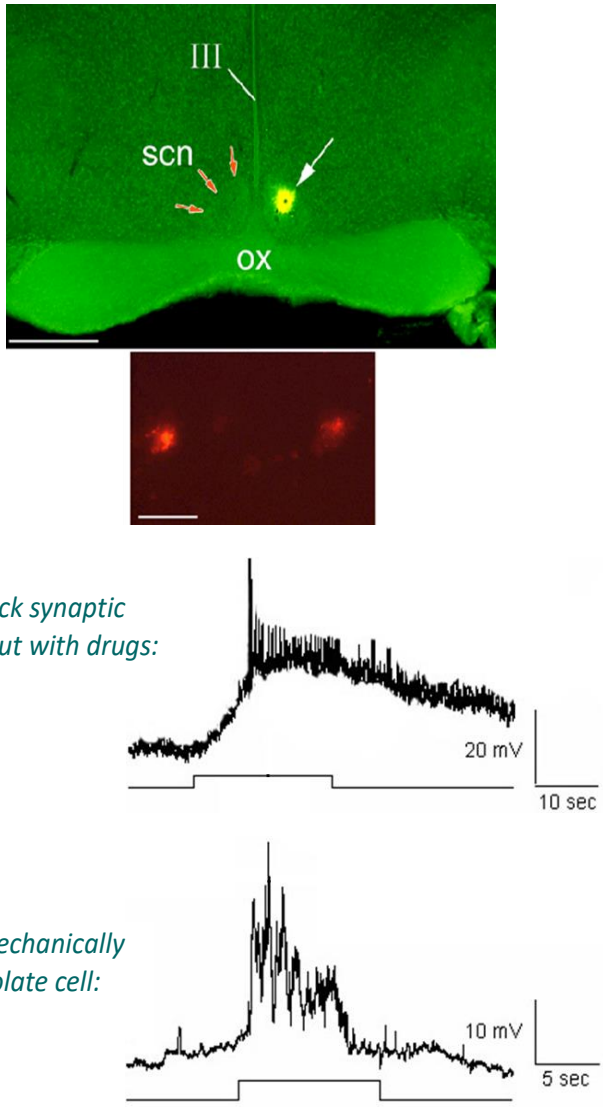

Figure 1.4: Labeling and light responses of rat ganglion cells innervating the SCN. *Top:* Fluorescent dye injected into the SCN. The red markers dictate the boundaries of contralateral SCN. *Middle:* Two ganglion cells from the SCN. *Bottom:* Light responses of SCN projecting ganglion cells in the presence of synaptic blockers and after cell has been isolated mechanically (Berson et al., 2002).

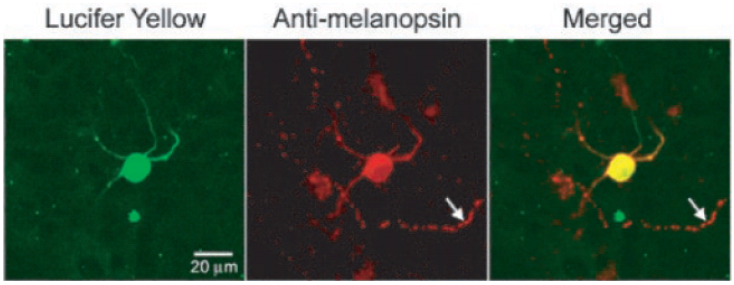

Figure 1.5: Immunolabeling of ipRGCs. Rat photosensitive ganglion cells were injected with Lucifer Yellow *(first panel)* and stained for melanopsin immunoreactivity *(middle panel).* Intrinsically photosensitive ganglion cells were melanopsin-positive *(last panel)* (Hattar et al., 2002).

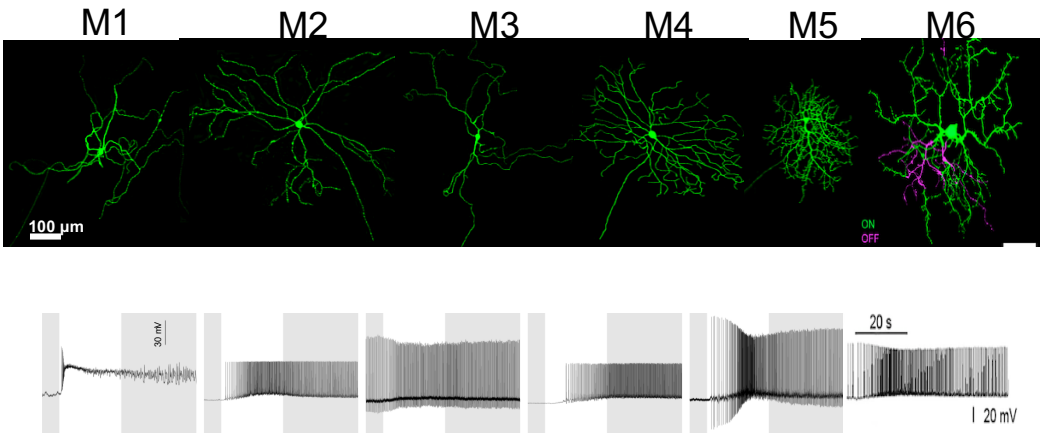

Figure 1.6: Morphological differences among M1-M6 type ipRGCs. Each ipRGC type is morphologically different and generates unique responses to light. *Top:* Five types have been identified in rat (M1-M5) (Reifler et al., 2015) and sixth type was been identified in mice (M6) (Quattrochi et al., 2019). *Bottom:* The data from the light responses are from Walch et al., 2015 (M1-M5) and from Quattrochi et al., 2019 (M6).

1.5 Synapses Within the Retina

Two types of synapses occur in neurons: chemical and electrical (Figure 1.7). When chemical synaptic transmission occurs, neurotransmitters are released from the presynaptic neuron into the synaptic cleft and bind to receptors on the postsynaptic neuron. However, in electrical synapses gap junctions allow ions to passively diffuse from one cell to a neighboring cell. In the mammalian retina, all major cell classes utilize electrical synapses as a way to transfer ions. It is important for interneurons to not only communicate via chemical synapses—the dominant mode of signal transmission—but also through electrical synapses to aid in encoding environmental stimuli. Electrical synapses are abundant across the nervous system and research has explored the unique characteristics of gap junctions including connexin makeup, conductance of cell-to-cell connectivity and effects of neurotransmitter modulation on neuronal coupling (Veenstra et al., 1994 a,b; Harris, 2001; Beyer et al., 2012). Gap junctions serve as an important mode for direct interneuronal communication between adjacent cells. This communication allows small molecules (typically less than 1000Da) such as ions and metabolites to be exchanged passively (Sohl et al., 2004; Sosinsky et al., 2005). Each cell contributes one hemichannel, also known as a connexon. Two connexons interact and form an intercellular channel (Segretain et al., 2004). Each connexon is comprised of 6 connexin (Cx) subunits (Sosinsky et al., 2005) (Figure 1.8). Connexins are evolutionarily conserved between species with at least 20 isoforms in humans (Sohl et al., 2004; Segretain et al., 2004; Sosinsky et al., 2005). There are numerous types of connexins, all of which can form a variety of connexons based on their sequence identity (α, β or γ) (Sohl et al. 2004). A homomeric connexon contains just one type of connexin, whereas a heteromeric connexon contains two or more types of connexin proteins. When a gap junction channel is formed by two connexons with the same

composition, it is called a homotypic channel, but when the channel is formed by two connexons with different compositions, it is called a heterotypic channel (Bloomfield & Völgyi, 2009).

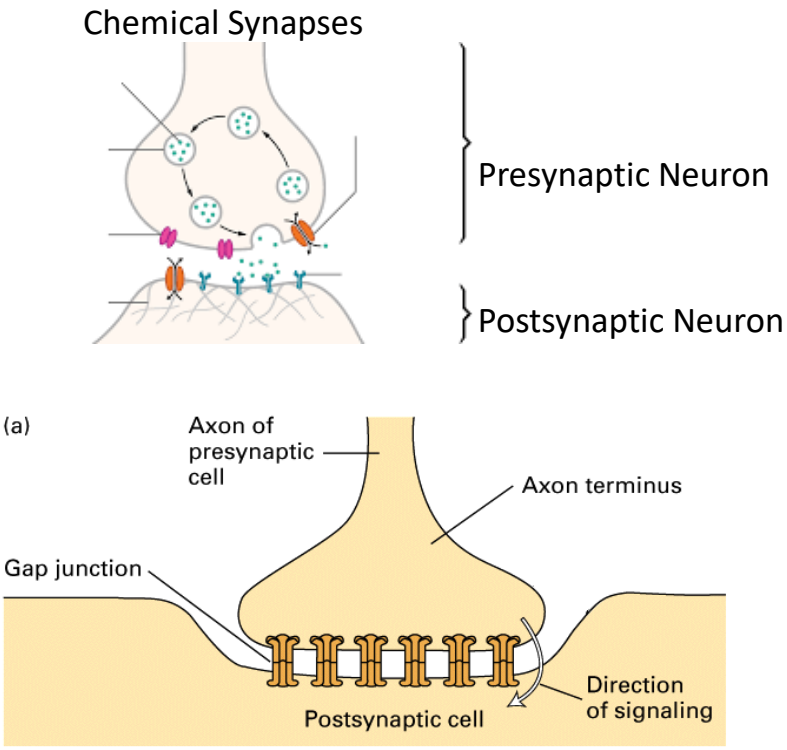

Figure 1.7: Schematic drawing of two synapses that occur between neurons. *Top:* chemical synapses via vesicle release of small chemicals. *Bottom:* electrical synapses via gap junctions (www.zoology.ubc.ua).

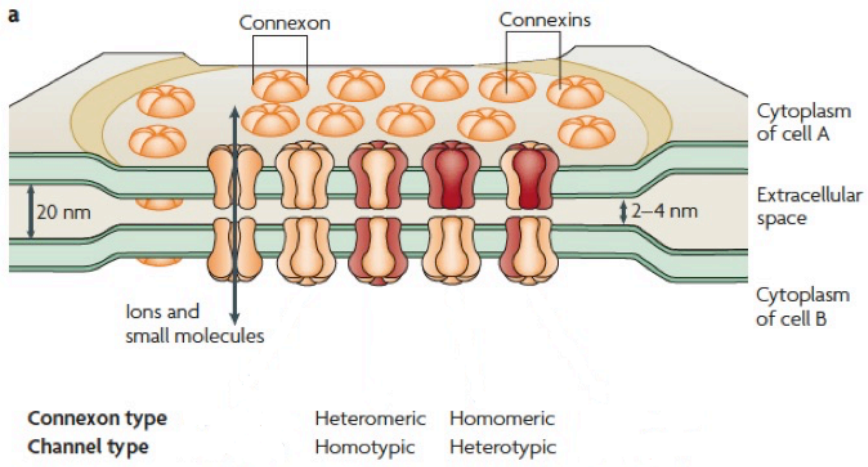

Figure 1.8: Schematic diagram of gap junction channel. Various types of channels formed by connexins between neighboring neurons (Bloomfield and Völgyi, 2009).

1.6 From the Retina to the Brain

The retina projects directly to image-forming and non-image-forming visual centers in the brain via ganglion cells, the output neuron of the retina. In humans, nearly 20 types of ganglion cells provide roughly 20 established parallel pathways leaving the retina and projecting primarily to the lateral geniculate nucleus of the thalamus (LGN). Roughly 20% of retinal ganglion cells (RGCs) in the mouse project to the LGN (Hattar et al., 2006; Ellis et al., 2016). Thalamic cells then project directly to primary sensory cortical areas which are responsible for processing information as sensory perception. Another major target of RGCs is the superior colliculus (SC), which is located below the thalamus. 90% of RGCs in the mouse project to the SC, an area known to control eye movements, detect novel objects in the visual scene, and evoke defensive behaviors in mice (Ellis et al., 2016). ipRGCs' axons project to both NIF and IF centers of the brain. Several of the axonal projections of ipRGCs to these centers are represented in the schematic below (Figure 1.9) (Hattar et al., 2006).

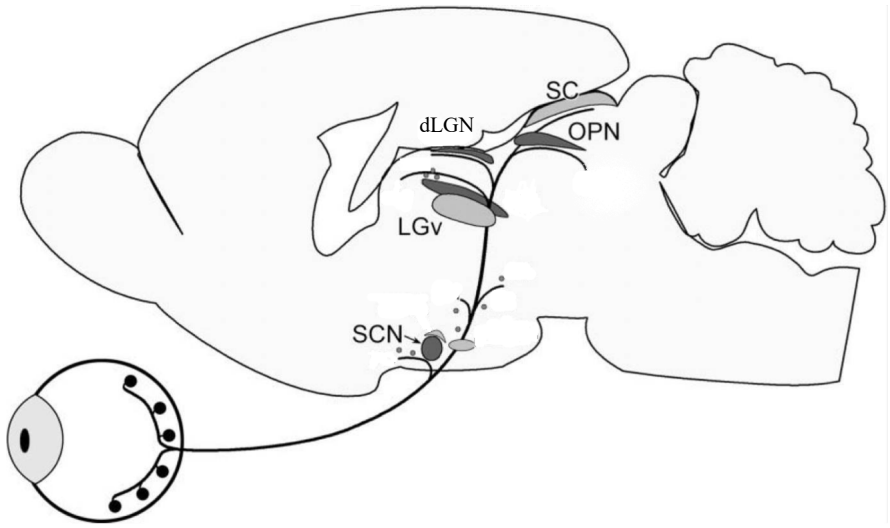

Figure 1.9: ipRGCs' axonal brain targets. ipRGCs' axon collaterals project mainly to non-image-forming (NIF) regions such as the suprachiasmic nucleus (SCN) and the ovillary prectal nucleus (OPN) as well as to image-forming (IF) brain regions namely the superior colliculus (SC) and the dorsal lateral geniculus nucleus (dLGN). Image modified from (Hattar et al., 2006).

1.7 Visual Impairment and Therapeutic Approaches

The discovery of melanopsin in ipRGCs now offers a mechanistic understanding of how light affects human physiology, behavior, sleep and NIF vision. Intraretinal ipRGC signaling to dopaminergic ACs and displaced ACs might form the basis for adaptation of the visual system to light intensity levels. In addition, innervations to the LGN by ipRGCs suggest the melanopsin system might directly transmit ambient light intensity information to the image forming visual system. There are several applications in which the melanopsin photosystem can have direct implications on human health and disease. For example, the human lens progressively loses the ability to detect blue range of visible light such that a 75-year-old detects less light at this wavelength than a 5-year-old. Therefore, it would be ideal to implant an intraocular lens in elderly patients that would allow for sufficient detection of blue light in order to restore proper stimulation of melanopsin, which is most sensitive to blue light.

Another use of melanopsin is in gene and mechanism discovery. A specific amino acid change mutation in melanopsin is associated with a small subset of patients with seasonal affective disorder (SAD) (Kawasaki and Kardon, 2007; Roecklein et al., 2012). SAD patients develop a form of depression that commonly begins with the short winter days and many patients find it helpful to improve alertness through light therapy, which uses intense light to strongly stimulate melanopsin. Furthermore, in industrial nations, the general population is often exposed to prolonged hours of artificial light that extends into the night, and nocturnal stimulation of ipRGCs can have harmful effects (Lucas et al., 2013; Vartanian and Wong, 2017). For example, most hospital facilities have 24-hour lighting, and this is now prompting light manufacturing companies and architects to adapt to dynamic lighting for the workplace. We have also seen

similar changes in technology as it relates to screen time usage. With the increase of technological advances, we are more prone to stay on our phones/computers for long durations. Social media has increased screen time by constantly keeping us connected to those we love and to information worldwide. Additionally, students from grade school to college are completing more homework assignments, which require them to use the internet for prolonged hours. To mitigate the potentially harmful effects of this increased light exposure, many consumer electronics allow users to decrease the blue light being emitted from the screen during nighttime hours to reduce melanopsin excitation.

Despite these advances to increase knowledge and understanding on melanopsin's function in order to improve human health, significant barriers still remain. A major knowledge gap is the mechanism behind ipRGC signaling to other neurons in the retina. It is my hope that this thesis helps uncover many of the unsolved questions within the field while gaining more insight into importance of ipRGC intraretinal signaling.

Chapter 2 Materials and Methods

2.1 Animals

Ethical approval

The University of Michigan Institutional Animal Care & Use Committee approved all experimental procedures. All mice tested in the following studies were at least 3 months of age and as old as 18 months. Both sexes were included, unless noted otherwise. Mice were housed on a 12-hour light 12-hour dark cycle with all experiments done during the light phase. All animals were genotyped by lab members Kwoon Wong, Andrew Chevernack, and Austra Lipia.

Chapter 3

Rd1/rd1 mice (Jackson Laboratory) are homozygous for retinal degeneration 1 mutation, resulting in the loss of all rods and ~97% of cones (Foster et al., 1991; Garcia-Fernandez et al., 1995; Freedman et al., 1999). *Rd12/rd12* mice (Jackson Laboratory) have a mutation in RPE65 and fail to convert all-trans retinal to 11-cis retinal; therefore, rod/cone function is attenuated (Pang et al., 2005). Experiments in this chapter used $rd1^{-/-}; rd12^{-/-}$ mice generated from crossing parents with the genotypes $rd1^{-/-}$, $rd12^{-/-}$ (i.e. both retinal degeneration 1 and RPE65 mutations). In these mice, rod/cone function is virtually completely abolished and thus ipRGCs are the only functioning photoreceptors.

Chapter 4

To selectively target ipRGCs, we used a melanopsin specific GFP expression line.

To produce *Opn4*$^{Cre/+}$::GFP animals, *Opn4*$^{Cre/Cre}$ mice were crossed with a Z/EG transgenic floxed GFP mouse line. Specifically in *Opn4*$^{Cre/Cre}$ mice, the melanopsin coding sequence is replaced by Cre recombinase in both alleles creating an *Opn4*$^{Cre/Cre}$ knock-in line (Hatter et al., 2008). The second line uses a Z/EG transgenic floxed GFP mouse line in which enhanced GFP (eGFP) is expressed under the b-actin promoter and CMV enhancer (Ecker et al., 2010, Jackson Laboratories) (see Figure 2.1 for generation of Z/EG mouse line from Ecker et al., 2010). The *Opn4*^{Cre} system allows for the manipulation of loxP-flanked target genes selectively in melanopsin-expressing cells (Hatori et al., 2008). These animals contain one copy of the melanopsin gene, with the other copy of the gene replaced by Cre recombinase which drives eGFP expression in cells where the melanopsin promoter is active, i.e. ipRGCs (Hatori et al. 2008; Ecker et al., 2010; Zhao et al., 2014).

In the ipRGC specific connexin36 (Cx36) knockout line (ipRGC-Cx36$^{flox/flox}$::GFP^{+}), *Opn4*$^{Cre/+}$Cx36$^{+/+}$::GFP$^{+/-}$ animals were crossed with a knock-in Cx36$^{flox/flox}$ line (*Opn4*$^{+/+}$Cx36$^{flox/flox}$::GFP$^{-/-}$) in which both copies of connexin36 gene are flanked by loxP sites. In the presence of Cre recombinase, the floxed gene is excised. The progeny with the following genotypes were genotyped and selected to continue crosses: *Opn4*$^{Cre/+}$Cx36$^{flox/+}$GFP$^{+/-}$ and *Opn4*$^{Cre/+}$Cx36$^{flox/+}$::GFP$^{-/-}$. These pups were then crossed to obtain the desired mouse line: *Opn4*$^{Cre/+}$Cx36$^{flox/flox}$::GFP$^{+/-}$. The results of this cross created the following mouse line, ipRGC-Cx36$^{-/-}$ in which all ipRGCs lack Cx36. In addition, all ipRGCs express GFP.

Previous labs have utilized the Cre-loxP system under the melanopsin promoter (Ecker et al., 2010; Estevez et al., 2012; Hu, Hill and Wong, 2013; Quattachi et al., 2019) and have shown that under the melanopsin promoter cells express GFP. As a caveat, Ecker et al. found that some cells were positive for melanopsin but showed no detectable level of GFP and they concluded that this phenotype was due to cells expressing insufficient Cre activity or GFP level (Ecker et al., 2010).

Chapter 5

The aim of this study was to explore changes that occur when all ipRGCs lack the NR1 subunit of NMDA glutamate receptors. *Grin1* is the gene responsible for activation of the NR1 subunit on NMDA receptors and therefore deleting this gene results in loss of NDMA receptor function. The Cre-loxP system was used to obtain this mouse line, in which the *grin1*$^{flox/flox}$ mouse line (Tsien et al., 1996) was crossed with *Opn4*$^{Cre/+}$::GFP mice. The results of this cross created the *ipRGC-nr1*$^{-/-}$::GFP^{+} mouse line in which all ipRGCs lack functional NMDA receptors and express GFP.

Chapter 6

Four mouse strains were used: 1) *Opn4*$^{Cre/Cre}$ mice ("melanopsin knockout mice") (Ecker et al., 2010), 2) *Gnat1*$^{-/-}$ mice with non-photosensitive rods (Calvert et al., 2000), 3) *Gnat2*^{cpfl3} mice with non-photosensitive cones (Chang et al., 2006), and 4) B6129SF2/J control mice (WT) made by crossing C57BL/6J with 129S1/SvImJ mice (Jackson Laboratory stock # 101045). Only male mice were used in this study to minimize the number of variables. In our initial observations, we noticed a slight difference in visual acuity measurements between male and female mice, but this slight difference subsided towards the end of testing. We decided

to proceed with only male mice.

2.2 Tissue Preparation

The ages of mice used ranged from 3 months to 1.5 years. Mice were dark-adapted overnight prior to experimentation in a ventilated lightproof box. Under dim red light, animals were euthanized using CO_2 inhalation followed by enucleation. All subsequent tissue preparation procedures were performed under infrared illumination using night vision devices (NiteMate NAV-3; Litton Industries, Watertown, CT, USA) attached to the eyepieces of a dissecting microscope. The retinas were harvested, dissected into quadrants and put in room temperature Ames' medium (Sigma; St Louis, MO, USA) that bubbled continuously with carbogen (95% O_2/ 5% CO_2). Each quadrant piece was mounted on a separate piece of 4" x 6" cellulose lens paper (Fisher Scientific) with the retinal ganglion cell (RGC) layer up for experimental purposes. Retinas were superfused at ~5ml/min with bicarbonate-buffered Ames medium and all experiments were completed at 32°C using a temperature controller (Warner Instruments, Hamden, CT).

2.3 Intracellular Injections

The ganglion cell layer was visualized through infrared transillumination and GFP-expressing cells were visualized using a x40 water-immersion objective and conventional FITC epifluorescence (blue excitation light) (Eclipse E600FN microscope, Nikon, Melville NY). Sharp glass microelectrodes (Sutter Instruments Company, Novato, CA) were pulled and back-filled

with a 4% Neurobiotin (Vector Laboratories), Lucifer Yellow (LY) (Electron Microscopy Sciences) and 1M KCl solution and typically had resistances between 100-145 MΩ. Cells expressing GFP were targeted for injection using a MultiClamp 700A amplifier (Molecular Devices, San Jose CA) to generate -1 to -3 nA pulses to iontophorese Lucifer Yellow. LY is too large to pass through retinal gap junctions. Once LY was visualized inside the soma of the targeted cell, successful penetration of the cells was confirmed, and the polarity of the current was switched to positive to favor the iontophoresis of the gap-junction permeable tracer, Neurobiotin.

The potential change in response to iontophoresis is given by Ohms's law as ΔV=Injection current * input resistance. Retinal cells do not survive potential differences greater than approximately +/- 1V so the iontophoresis injection current was decreased as input resistance increased (Table 2.1). Neurobiotin was injected into the targeted cell for 15 minutes. After successful injection of 3-4 GFP-labelled cells, the retina was removed from the chamber and placed in 4% paraformaldehyde (PFA) for 15 minutes followed by three 10-minute washes in phosphate-buffered saline (PBS) before immunostaining.

Membrane Resistance (R_M)	Current (I) injected
<300 MΩ	3nA
300-400 MΩ	2.5nA
400-500 MΩ	2nA
500-600 MΩ	1.5nA
>600 MΩ	1nA

Table 2.1: Current injection based on an individual cell's resistance.

2.4 Light Induced c-Fos Expression

Mice were dark-adapted at 6PM and continued dark adaptation overnight prior to experimentation in a ventilated lightproof box. All experiments were conducted during the 12:12 hour light cycle and mice were presented the light stimulation no earlier than 10am. Mice were placed in a clear cage and given food and water during the duration of the light stimulation. To induce maximum *c-fos* levels, a bright blue light (~16.0 log photons $cm^{-2}s^{-1}$) was presented to the entire cage continuously for 3 hours. Every 10 minutes, a light tap was made on the cages to encourage mice to remain awake. Following light exposure, mice were prepared for whole animal perfusion.

After each mouse had been exposed to 3 hours of bright blue light, it was placed in an enclosed apparatus in which it inhaled a mixture of 4% isoflurane and 2% oxygen until completely under anesthesia. 15mL of PBS was perfused into the animal and then 15mL of 4% PFA was perfused.

Once PFA had been perfused, the eyeballs were removed by carefully cutting the muscles and optic nerve attached to the eyeball and placed in a well containing 4% PFA for 30 minutes. After 30 minutes of incubation, each eyeball was washed in PBS three times for 10 minutes before they were placed in a jar filled with PBS for storage before retina dissection.

Under a 10x light microscope, the eyeballs were placed in a dish containing PBS and the retina was harvested using dissecting scissors. Once the retina was dissected, it was then cut into dorsal, ventral, temporal and nasal quadrants and later prepared for immunostaining (Sondereker et al., 2018).

2.5 Immunostaining

Neurobiotin injected ipRGCs

To visualize Neurobiotin, retinas were blocked with 10% normal donkey serum (NDS) and 2% triton X-100 solution for 2 hours at room temperature. For 5 days at 4°C, retinas incubated in the aforementioned primary blocking solution, with Streptavidin 568 (1:250) (Invitrogen Thermofisher Scientific). Retinas were then washed in PBS for 40 minutes before incubating in 5% NDS, 0.5% triton X-100 and Streptavidin 568 (1:250) solution overnight at 4°C. After the final washes with PBS, retinas were mounted in VECTASHIELD mounting medium (Vector). To prolong storage, coverslips were sealed, and slides were stored at 4°C in a slide box protected from light.

Previous work by Muller et al (Muller et al., 2010) incubated retinas in streptavidin-FITC or streptavidin-Cy3 in 0.3% triton X-100 overnight and visualized a small number of coupled cells. We increased the concentration of triton X-100 as well as extended the incubation period to maximize the time streptavidin has to bind to Neurobiotin. We found that incubating retinas longer than 5 days did not increase the average number of ipRGC-coupled ACs.

ipRGC-coupled amacrine cells

To visualize amacrine cells coupled to ipRGCs via gap-junctions post NB injection, retinas underwent the same protocol mentioned in the section above. Retinas were blocked with 10% normal donkey serum (NDS) and 2% triton X-100 solution for 2 hours at room temperature. For 5 days at 4°C, retinas incubated in the aforementioned primary blocking solution, with Streptavidin 568 (1:250) (Invitrogen Thermofisher Scientific). In some experiments, one or two of the following antibodies were also added to the primary block solution: rabbit anti-RNA-binding protein with multiple splicing (RBPMS; 1:500; PhosphoSolutions, Aurora CO); rabbit anti-GABA (1:250; MilliporeSigma); donkey anti-choline acetyltransferase (ChAT; 1:500; MilliporeSigma); mouse anti-nitric oxide synthase derived from brain (bNOS; 1:400; MilliporeSigma); rabbit anti-neuropeptide Y (NPY); 1:1000; Cell Signaling Technology, Danvers MA); rabbit anti-serotonin (1:250; ImmunoStar, Hudson WI); and sheep anti-vasoactive intestinal peptide (VIP; 1:250; Millipore). To visualize these primary antibodies, one of the following secondary antibodies (all from Jackson Immuno Research, West Grove, PA) was added to the above secondary block solution: donkey anti-rabbit FITC (1:250), donkey anti-mouse Cy3 (1:250), and donkey anti-goat Cy3 (1:250). Retinas were then washed in PBS for 40 minutes before incubating in 5% NDS, .5% triton X-100 and Streptavidin 568 (1:250) solution

overnight at 4°C. After the final washes with PBS, retinas were mounted in Vecta-shield mounting medium (Vector). To prolong storage, coverslips were sealed, and slides were stored at 4°C in a slide box protected from light.

To enhance serotonin immunostaining, injected retinas were kept in a separate dish containing Ringer's solution and remained in constant darkness. At the ed of the injection experiment, retinas were transferred to a new Ringer's solution containing serotonin at a concentration of 250ng/mL. Retinas were allowed to incubate for 30-60 minutes in the dark before proceeding with fixation. This prolonged incubation allowed amacrine cells to replenish their stores of serotonin which could have been releases due to light exposure during injection of ipRGCs.

Visualizing light induced c-fos expression

A ganglion cell specific marker, RNA- binding protein with multiple splicing (RBPMS) (Rodriguez et al., 2014), was used to visualize *c-fos* positive RGCs. Since *rd1; rd12* mice lack functional rod/cone photoreceptors, all *c-fos* positive RGCs can be assumed to be ipRGCs. Retinas were blocked with 10% normal donkey serum (NDS) and .5% triton X-100 solution for 2 hours at room temperature. For 5 days at 4°C retinas incubated in the primary blocking solution mentioned above with rabbit anti-RBPMS (1:500) (PhosphoSolutions) and mouse anti- *c-fos* (1:700) (Invitrogen Thermofisher Scientific). Retinas were washed in PBS for 40 minutes before incubating in 5% NDS, .5% triton X-100 and secondary antibodies Donkey anti-rabbit FITC (1:250) and Donkey anti-mouse Cy3 (1:250) solution overnight at 4°C. After the final washes with PBS, retinas were mounted in Vecta-shield mounting medium (Vector). The above-mentioned protocol to prolong storage was used after mounting retinas.

In some *c-fos* immunostaining experiments, the rabbit anti-RBPMS antibody was replaced by rabbit anti-nNOS (1:300) (Invitrogen Thermofisher Scientific) to determine whether some *c-fos* positive neurons in the ganglion cell layer of *rd1; rd12* retinas expressed neuronal nitric oxide synthase. This enzyme should be expressed only in ACs containing the neuromodulator nitric oxide, but not in RGCs.

2.6 Imaging and Analysis

Intracellular injections

Images were acquired using a Leica SP5 laser scanning confocal microscope with 20x objective. The intensity and contrast of the final images were adjusted in Adobe Photoshop. Each type of ipRGC, M1-M6, was classified and identified by examining the soma-size and dendritic stratification in the inner plexiform layer (IPL) based on previously reported characterizations for M1-M6 type ipRGCs (Hattar et al., 2006; Schmidt et al., 2008; Muller et al., 2010; Quattrochi et al., 2019). Once the ipRGC type was identified, the number of streptavidin positive somas around each injected ipRGC was manually counted and the average number of coupled cells per ipRGC type were analyzed and compared. Coupled cells were identified and included based on two parameters. The first parameter was verifying the shape of the cell (round-like or oval-like) which helped us differentiate between coupled cells and background staining. The second parameter was examining the location of the coupled cell (e.g. near the dendrite of the injected ipRGC). If the cell didn't meet this set of criteria, then it was excluded from analysis.

Additionally, the soma-diameter of the coupled cell was measured against the longest axis and categorized into three bin categories: 5um (2.5um-7.5um), 10um (7.6um-12.5um), and 15um (12.6um-17.5um). Average values are given as the mean ± S.E.M. and were compared using post-hoc statistical analysis.

c-fos induced ipRGC-coupled cells

Similar to the methods used to analyze cells stained by intracellular injections, images were acquired using a Leica SP5 laser scanning confocal microscope with 20x objective. The intensity and contrast of the final images were adjusted in Adobe Photoshop. ipRGCs were identified if cells were both *c-fos*- positive and RBPMS positive. In contrast, ACs were identified if they were *c-fos*- positive and RBPMS negative. After *c-fos*-positive cells have been identified as either ipRGCs or ipRGC-driven ACs, differences between dorsal, ventral, nasal and temporal regions were made.

2.7 Visual Behavior

The virtual optokinetic system (Prusky et al., 2004) manufactured by CerebralMechanics (Lethbride AB, Canada) was used. One at a time, before each session, mice were individually placed inside the arena on a platform surrounded by four three-dimensional computer monitors (Figure 2.1). Afterwards, the lid of the arena was closed, and the mouse was allowed to move freely on the platform. The genotype of the mouse was unknown prior to and during data collection and initial analysis. During testing, each computer monitor displayed a vertical sine

wave grating which drifted either clockwise or counterclockwise. As the stimulus moved in either direction, the mouse's tracking behavior was assessed.

Three parameters were tested: spatial frequency, drift speed, and contrast. For both spatial frequency and drift speed, the initial grating assessed had a low spatial frequency (e.g. 0.15 cyc/deg) and contrast of 100%. Each time the mouse was able to detect the rotating stimulus, the program increased the spatial frequency value. For drift speed, similar parameters were used as described above; however, the speed at which the stimulus rotated varied. Four drift speeds were tested: 8, 12, 16 and 20 deg/sec. The contrast threshold was calculated using Michelson contrast: (max luminance – min luminance) / (max luminance + min luminance). Finally, contrast sensitivity was defined as the reciprocal of the contrast threshold. At 100% contrast, the behavior indicated that the mouse saw clear black and white strips; but, as the contrast value decreased (e.g. 15%), the mice saw a "grayish" appearance from the stripes. Contrast threshold was identified at four spatial frequencies: 0.042, 0.092, 0.192, and 0.272 cyc/deg. Pairwise statistical comparisons were made using the Mann-Whitney U test and p-values smaller than 0.05 indicated significant differences.

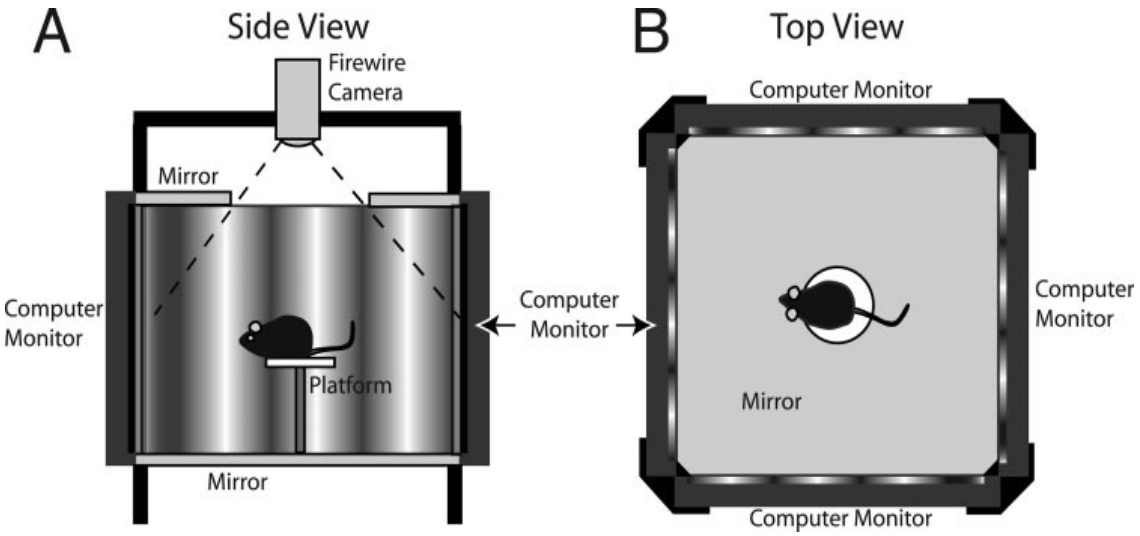

Figure 2.1: Schematic representation of the optomotor testing apparatus. *A) Side view.* A mouse is placed on a platform position in the middle of an arena. A video camera is used to monitor the animal's behavior to the rotating stimulus *B) Top view.* The mouse is enclosed by 360° of gratings which rotates clockwise or counterclockwise and the mouse is allowed to move freely on the platform (Prusky et al., 2004).

Chapter 3 Distribution of ipRGC coupled Amacrine Cells Across the Retina

3.1 Abstract

Within the mammalian retina there are more than 60 different types of neurons, each playing a specific role in visual processing (Masland, 2001). Scientists have examined the assortment of types of ganglion cell and ACs in mice in great detail (Dräger et al., 1981; Jeon et al., 1998; Masland, 2001, 20012; Valiente-Soriano et al., 2014; Muller et al., 2017). The highest density of ganglion cells (> 8000 cells/mm^2) was reported in the temporal region (Dräger and Olsen, 1981) and similarly, the highest density of ipRGCs was also reported in the temporal region (Valiente-Soriano et al., 2014). In contrast, the dorsal region of the retina contained the lowest density of ganglion cells (<2,000 cells/mm^2) (Dräger and Olsen, 1981). It was also reported that of the average number of cells in the ganglion cell layer (GCL), 41% are ganglion cells (3,300 cells/mm^2) while displaced ACs make up the remaining 59% of cells in the GCL (Jeon et al. 1981). While the density of both ganglion cells and ACs have been reported, the distribution of ipRGC-coupled ACs across the mammalian retina remains unexplored. Using immunocytochemistry techniques to identify the distribution of ipRGCs verses ipRGC-coupled amacrine cells, we found that there are more ipRGC-coupled ACs than ipRGCs in the nasal, ventral, and dorsal regions of the mammalian retina. In contrast, the temporal region has more ipRGCs than ipRGC-coupled ACs. Finally, we observed less than 5% of nNOS ACs that presumably coupled to ipRGCs.

3.2 Introduction

It was groundbreaking when scientists found that mice lacking rod and cone photoreceptors were still able to respond to environmental irradiance (Lucas et al. 1999; Freedman et al., 1999) and the primary candidate mediating these responses was ganglion cell photoreceptors (Berson et al., 2002; Hattar et al., 2002). As work continued to emerge, the exploration of light-induced genes in retinal neurons sparked a new wave of experiments. In response to light, an immediate-early gene, *c-fos,* is expressed in cells located in the ganglion cell layer (GCL) and inner nuclear layer (INL) of rodents (Sagar & Sharp, 1990; Koistinaho & Sagar, 1995; Heurta et al., 1997). Semo et al (Semo et al., 2003) showed that, in mice lacking rods and cones, c-Fos immunostaining is undetectable in dark-adapted conditions. In contrast, photostimulation induces robust c-fos expression in ipRGCs (but not other RGCs) and dopaminergic ACs that receive ipRGC input, indicating that c-fos immunostaining is a reliable method for detecting ipRGCs and ipRGC-driven ACs in rodless/coneless retinas.

A representation of the visual space is highly dependent on the arrangement of ganglion cells and their distribution throughout the retina. The distribution of mouse ganglion cells was studied using retrograde filling with horseradish peroxidase. Results from Drager and Olsen identified 70,000 ganglion cells located in the ganglion cell layer of the mouse retina and the greatest density of these cells (8,000 cells/mm^2) were temporal to the optic disk while ganglion cells located in the dorsal retina were less dense (2,000 cells/mm^2) (Dräger and Olsen, 1981). More recently, the ipRGC population and distribution was examined in pigmented mice using either

melanopsin antibodies or Brn3a as a marker for ipRGC identification (Jain et al., 2012; Hughes et al., 2013; Valiente-Soriano et al., 2014). They concluded that there are roughly 1,100 ipRGCs in the mouse retina (Jain et al., 2012; Valiente-Soriano et al., 2014), however Hughes et al reported higher numbers, around 1,800 (Hughes et al., 2013). It was suggested that the differences in total population were due to a higher concentration of antibody used to detect ipRGCs; however, Berson et al. reported nearly 2,570 ipRGCs in pigmented mice and estimated that the total number of ipRGCs was based on the assumption that ipRGCs are equally distributed across the retina (Berson et al., 2010). Additional studies from Valiente-Soriano et al, Hughes et al, and Jain et al, concluded that contrary to the assumption of Berson et al., ipRGCs were more abundant in the temporal region of the retina.

ACs are the most diverse group of neurons in the mammalian retina (Masland 2001, 2012). Within the mouse INL, they comprise more than 30% of cells (Jeon et al., 1998) and make up ~60% of cells located in the GCL (Jeon et al., 1998). Using Prox1 as a marker for neuronal expression, Muller et al found that Prox1-immunoreactive AII amacrine cell bodies were located in all regions of the retina and there were no significant differences between the different retinal quadrants (Muller et al., 2017). ACs can be distinguished by their soma size, dendritic field sizes, dendritic stratification levels and neurotransmitter and/or neuromodulator content.

The studies mentioned above have shown light-induced *c-fos* expression is dependent on multiple factors including the age of mice (Semo et al., 2003), and the duration of light presented (Nir & Agarwal, 1993). Moreover, after light exposure the expression levels of *c-fos* –positive cells are different between cells located in the GCL and cells located in the INL (Sagar & Sharp,

1990; Koistinaho & Sagar, 1995; Heurta et al., 1997; Hughes et al., 2016). Furthermore, while additional studies revealed that the distribution of ganglion cells, ipRGCs and ACs are quite different in the mammalian retina (Dräger and Olsen, 1981; Jeon et al., 1998; Berson et al., 2012; Jain et al., 2012; Hughes et al., 2013; Valiente-Soriano et al., 2014; Muller et al., 2017) what remains unclear is the distribution of ipRGC coupled amacrine cells across the mouse retina. To fill in this knowledge gap, a bright blue light was presented to *rd1*$^{-/-}$*; rd12*$^{-/-}$ mice, which lack rod and cone function, for 3 hours to induce c-Fos expression in ipRGCs and ipRGC-driven amacrine cells. Using this method, we compared c-Fos positive amacrine cells to c-fos positive ganglion cells in 4 retinal quadrants: dorsal, ventral, temporal and nasal.

3.3 Results

To understand how ipRGC-coupled amacrine cells are distributed across the mammalian retina, we used a mouse line in which rod and cone photoreceptors are functionless and presented mice with a bright blue light to induce c-Fos expression. After euthanasia, retinas were fixed with PFA and stained with anti-rabbit RBPMS (visualized with a FITC-tagged secondary antibody), a ganglion cell marker, and anti-mouse c-Fos (visualized with a Cy3-tagged secondary antibody). Retinas (n=5) were cut into four quadrants: dorsal, ventral, temporal and nasal as described from Sondereker et al (Sondereker et al., 2018). From the confocal images captured, we counted c-Fos –positive and RBPMS-positive somas which indicated ipRGCs, while c-Fos –positive (Figure 3.1 and Figure 3.2) and RBPMS-negative somas were identified as ipRGC-coupled amacrine cells (Figure 3.2). Therefore, the percentage of ipRGC-coupled amacrine cells per quadrant is derived from the c-Fos –positive /RBPMS-negative somas in the GCL as a fraction of the total c-

Fos –positive cells. Additionally, we examined the differences in densities between ipRGCs and ipRGC-coupled amacrine cells. The density of ipRGCs and ipRGC-coupled amacrine cells was calculated by dividing the number or cells in the field (ipRGCs or ipRGC-coupled amacrine cells) by the area of that field of view.

In the dorsal region of the retina, a total of five pieces were analyzed and c-Fos –positive cells were mostly amacrine cells (56.16%, n=196 cells) compared to 43.83% (n=153 cells) of ganglion cells (presumably ipRGCs); therefore within this quadrant, the density of amacrine cells (30.25 cells mm^{-2}) is greater than the density of ipRGCs (21.71 cells mm^{-2}). Similar to the dorsal region, in the ventral (n=4 pieces analyzed) and nasal (n=1 piece analyzed) regions, the majority of c-Fos –positive cells were identified as amacrine cells (ventral: 79.8%, n=162 cells; nasal: 61% n=25 cells) and the density of amacrine cells (ventral: 87.82 cells mm^{-2}; nasal: 45.60 cells mm^{-2}) was greater than the population of ipRGCs (ventral: 17.16 cells mm^{-2}; nasal: 29.10 cells mm^{-2}). In contrast, more c-Fos –positive cells were identified as ganglion cells (80.9%, n=132 cells) than amacrine cells (19%, n=31 cells) in the temporal region (n=5 pieces analyzed) and therefore, ganglion cells are denser in this region compared to the other 3 regions (49.84 cells mm^{-2}) (Figure 3.3).

As a negative control, we kept a mouse (n=1) in constant darkness for three hours and after euthanasia, retinas were fixed as described above and stained with anti-mouse c-Fos (visualized with 488-tagged secondary antibody). In the negative control retinas, a total of 4 pieces (dorsal n=2 and ventral n=2) were analyzed and the cell densities were calculated. In the dorsal region of the retina, the average density of c-Fos positive cells (8.00 cells/mm^{-2}, S.E.M. 0.974) and the

average density of c-Fos positive cells in the ventral region of the retina (13.14 cells/mm^{-2}, S.E.M. 2.59). Although we noticed a few cells c-Fos positive cells (figure 3.1), this response could have resulted from transporting the mouse from one experiment room to another for euthanasia via perfusion and therefore was not due to light exposure during the 3 hours of constant darkness.

Previous work from Reifler et al reported that ipRGCs are electrically coupled to three types of amacrine cells 1) monostratified cells, 2) bistratified cells, and 3) polyaxonal cells and their ipRGC-driven light responses were ON sustained (Reifler et al., 2015). Four years later, Jacoby et al characterized the morphology of nitric oxide (NO) containing amacrine cells (Jacoby et al., 2019). Similarly, the morphology of the NO containing amacrine cell resembled the morphology of the polyaxonal amacrine cell that Riefler et al reported receiving input from ipRGCs (Reifler et al., 2015). We therefore wanted to test the hypothesis that some nNOS amacrine cells are ipRGC-coupled. Retinas were stained with anti-mouse c-Fos (visualized with a Cy3-tagged secondary antibody) and anti-rabbit-nNOS (visualized with a FITC-tagged secondary antibody). In two out of three quadrants analyzed, we found less than 5% of ipRGC-driven amacrine cells were nNOS positive (6/132 cells) (Figure 3.4). There were no ipRGC-driven nNOS-positive amacrine cells located in the ventral region of the retina and no data was taken from the nasal region of the retina. The majority of these cells were located in the GCL of the retina and within the temporal and dorsal regions. Out of 17 ipRGC-coupled amacrine cells in the temporal region, 2 were ipRGC-driven nNOS-positive. Among the 50 ipRGC-coupled amacrine cells in the dorsal region, 4 were nNOS-positive.

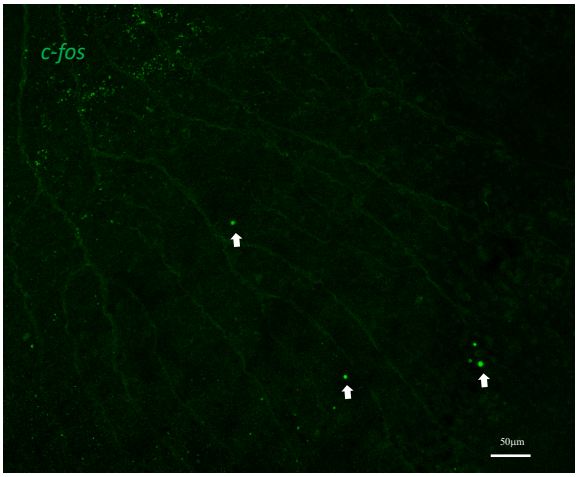

Figure 3.1: c-Fos expression in dark adapted retinas. Confocal image of c-Fos positive cells (ipRGCs) stained cells located in the dorsal region of the mammalian retina from a dark adapted *rd1; rd12* mouse. White arrows indicate c-Fos positive cells (ipRGCs). Scale bar = 50µm.

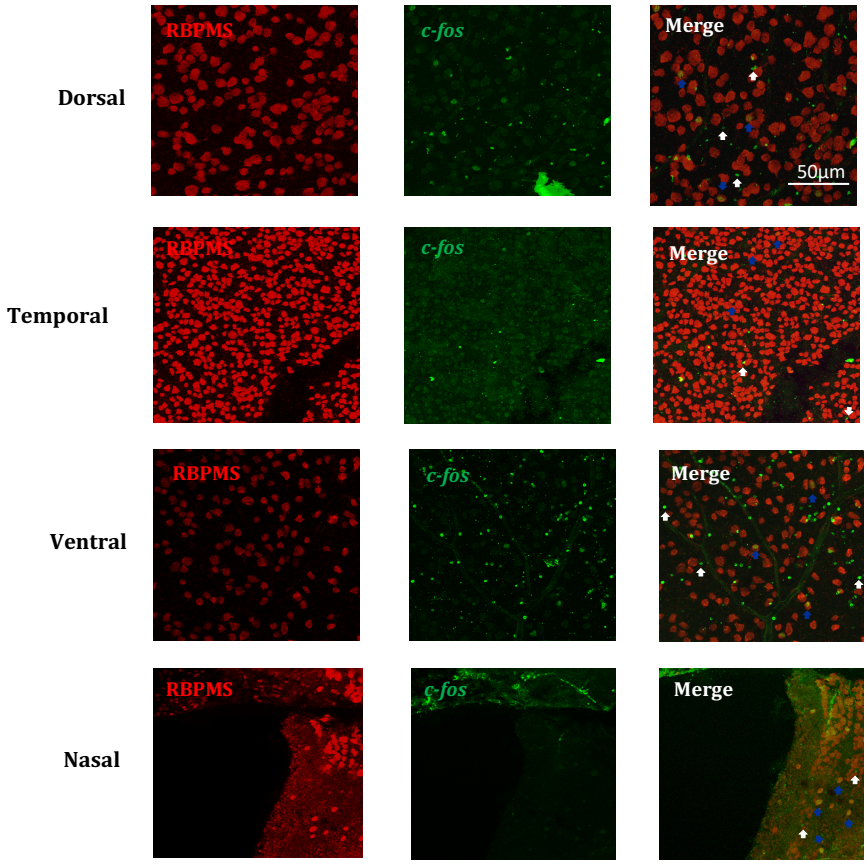

Figure 3.2: Confocal images of ipRGC-coupled ACs and ipRGCs. Images of ipRGCs and ipRGC-driven amacrine cells were stained and located in the dorsal, ventral, temporal, and nasal regions of the mammalian retina from *rd1; rd12* mice. White arrows indicate ipRGCs while blue arrows indicate ipRGC-driven amacrine cells. Scale bar = 50µm.

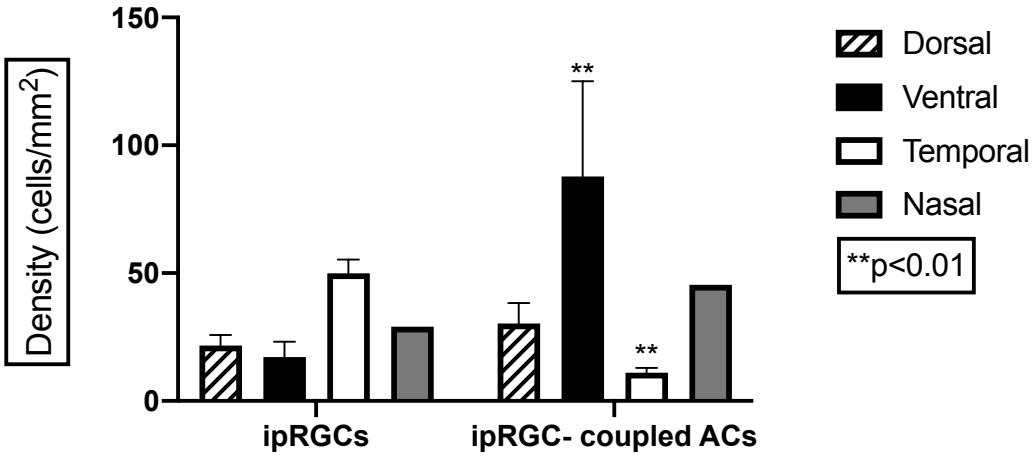

Figure 3.3: Comparative distribution between ipRGCs and ipRGC-coupled ACs. The density of ipRGCs and ipRGC-coupled ACs were calulated in the dorsal, ventral, temporal and nasal quadrants across the mammalian retina. Data generated from *rd1; rd12* mice.

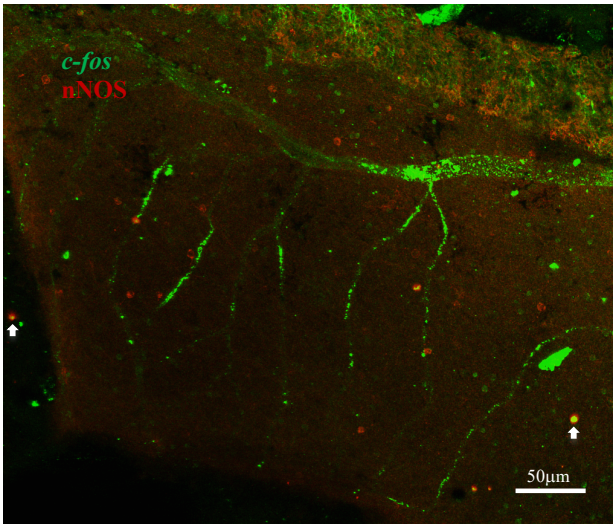

Figure 3.4: ipRGC-coupled amacrine cells contain nNOS. ipRGC-driven amacrine cells are nNOS immunopositive (cfos-posive (FITC) and nNOS-positive (Cy3)), denoted by arrow heads. Confocal image taken from the dorsal region of the mammalian retina. Scale bar = 50um.

3.4 Discussion

This study gained insight into the distribution and density of ipRGC-coupled amacrine cells within various quadrants of the mammalian retina. We showed that in *rd1*$^{-/-}$*; rd12*$^{-/-}$ mice, ipRGCs are densely located in temporal region of the retina. Our findings are consistent with the previously reported ipRGC distribution findings from Valiente-Soriano et al (Valiente-Soriano et al., 2014). Additionally, Hughes et al. reported that between the dorsal and ventral regions, melanopsin-positive cells were higher in the dorsal region of the retina, specifically M1- and M2-type ipRGCs while the ventral region, M4-M5-type ipRGCs were intensely stained (Hughes et al., 2013). Similarly, we also found that there were more ipRGCs located in the dorsal region compared to the ventral region. We did not examine how each type of ipRGC is distributed across the retina.

Using an antibody to detect nNOS-containing amacrine cells, we showed that a few ipRGC-driven amacrine cells contained nNOS. Nitric oxide (NO)-containing amacrine cells contain an enzyme, NOS, that synthesizes NO from L-arginine. Although amacrine cells form synapses only within the inner plexiform layer, the neuromodulators they secrete are thought to diffuse over great distances and affect all five classes of retinal neurons in a paracrine manner. Presumably, in response to photostimulation, ipRGCs transmit their excitatory light responses to NO-containing amacrine cells via gap junction, which causes these interneurons to secrete NO that could potentially exert a variety of modulatory effects throughout the retina. While the effects of NO release have been extensively studied in the brain and have been known to contribute to neural processing and neurovascular coupling, within the retina, the release of NO

within the retina has begun to change the way we understand how neuromodulators regulate retinal circuits.

Within the turtle inner retina, nNOS was found localized at presynaptic terminals of amacrine cells and synthesis of NO was shown to impact neurotransmitter release (Cao and Eldred, 2001). Additionally, NO release impacts gap junction conductance between AII amacrine cells and cone bipolar cells (Mills and Massey, 1995), regulates the temporal response properties of OFF bipolar cells (Vielma et al., 2014), regulates the release of GABA and glycine from amacrine cells (Yu and Eldred, 2005), and even modulate the responses of ON and OFF RGCs (Wang et al., 2003). Mills and Massey identified one of the first targets of NO signaling on the Cx45 side of the hetero-junctions between AII ACs and ON cone bipolar cells (Mills and Massey, 1995) and it was later shown that mice lacking NO demonstrated defects in their ability to detect light responses, synthesize and produce NO (Wang et al., 2007). In the mammalian retina, nNOS expressing amacrine cells are homogenously coupled to each other and are responsible for releasing NO upon light-induced depolarization throughout the inner retina (Jacoby et al., 2018). While NO release has been shown to increase presynaptic vesicle fusion and GABA release, it was not dependent on action potentials and had no effect on postsynaptic receptors but instead relied upon cytosolic Ca^{2+} (Maddox and Gleason, 2017). It would be of interest to learn whether signaling from ipRGCs to nNOS amacrine cells induces any of these modulatory effects of NO.

As mentioned in the Results section, 5% of nNOS-immunopositive cells are ipRGC-coupled amacrine cells, while the rest are presumably nNOS amacrine cells that receive input from rod/cone circuits. We predict that the former population generates sustained light responses,

whereas the latter cells generate more transient responses since the Wong lab previously showed that ipRGCs' photoresponses are far more sustained that all other RGCs' (Wong et al., 2012), and that amacrine cells receiving input via gap junctions likewise exhibit very sustained photoresponses (Reifler et al., 2015). The sustainedness of these amacrine cells' light responses probably enables them to stably encode the absolute ambient light intensity.

Chapter 4 Tracer Analysis of ipRGC-coupled Amacrine Cells

4.1 Abstract

Since their discovery, significant advances in our understanding of the roles ipRGCs play in vision have expanded. It has become clear that ipRGCs' axon project to several image-forming visual nuclei in the brain (Hattar et al., 2006), including the dorsal lateral geniculate nucleus, and the superior colliculus (Ecker et al., 2010). In addition to their role in both non-image and image forming vision, ipRGCs transmit their light-evoked responses to displaced amacrine cells (ACs) via gap junctions as evident by electrophysiology (Reifler et al., 2015) and tracer injections (Muller et al., 2010). Previously published work showed that ganglion cell to amacrine cell coupling primarily is dependent on connexin 36 (Cx36) and connexin 45 (Cx45) (Pan et al., 2010; Pang et al., 2013). Here we extend the previous reports by showing that each of the six types of ipRGCs (M1-M6) can be tracer-coupled to ACs located in the ganglion cell layer (GCL) of the retina. Furthermore, we show preliminary analysis categorizing the coupled amacrine cells, by examining the soma diameter of each cell. We also report that Cx36 contributes to ipRGC-AC coupling.

4.2 Introduction

To date, six types of ipRGCs, M1-M6, have been discovered in mice, along with five types in rats (Berson et al., 2002; Viney et al., 2007; Schmidt et al., 2008; Ecker et al., 2010; Brown et al., 2012; Zhao et al., 2014; Riefler et al., 2015; Quattrochi et al., 2019). Researchers sought to explore the photo-diversity amongst each type, in addition to uncovering their potential involvement in image-forming vision (Hattar et al., 2003; Viney et al., 2007; Schmidt et al., 2008; Ecker et al., 2010; Brown et al., 2012; Zhao et al., 2014; Riefler et al., 2015; Quattrochi et al 2019). Through the use of genetically encoded fluorescent proteins (Hatter et al., 2002; Ecker et al., 2010), whole-cell recordings (Wong et al., 2007; Zhao et al. 2014; Reifler et al., 2015; Wong et al., 2017; Quattrochi et al., 2019), retrograde labeling (Berson et al. 2002), calcium imaging (Sekaran et al., 2003; Bramley et al., 2011) intracellular injections (Muller et al., 2010) and behavioral studies (Ecker et al., 2010; Estevez et al., 2012; Schmidt et al. 2014; Alam et al., 2015; Schroeder et al., 2018) researchers have uncovered critical new information which identifying the dendritic stratifications of M1-M6 type ipRGCs, new axonal targets, spatial differences in response to various light intensities, and ultimately the contributions of ipRGCs in visual function.

It is now clear that ipRGCs innervate image-forming brain regions in addition to their role in non-image-forming (NIF) functions. In 2008, it was found that ipRGCs can signal intraretinally by transmitting their light-evoked signals to dopamingeric amacrine cells by AMPA/kainate glutamate receptors (Zhang et al., 2008); and in 2015, researchers revealed that displaced ACs receive gap-junction input from melanopsin ganglion cells (Reifler et al., 2015). To further explore ipRGC-AC coupling, researchers utilized a technique in which an intracellular tracer dye

was injected into fluorescently labeled ipRGCs. The gap-junction permeable molecule was allowed to diffuse into the coupled cells and the results showed that M1-M3 type ipRGCs are gap-junction coupled to multiple amacrine cells (Muller et al., 2010).

At electrical synapses, gap junctions allow neighboring cells to communicate and ions can passively diffuse from one cell to another. Multiple gap junction proteins in the mouse retina participate in electrical signaling (Schubert et al., 2005). Specifically, connexin 36 (Cx36) and connexin 45 (Cx45) are abundantly expressed in the synaptic layers (Dedek et al., 2006). Therefore, to study the neuronal role of these connexins, one successful strategy has been to use a transgenic mouse line with Cre under an appropriate promoter to knock out these connexins only in neurons of interest (Maxeiner et al., 2005).

Connexin36 is expressed at the gap junctions of ACs, most ganglion cells and rod and cone cells; Cx45 is expressed in ACs, ON cone bipolar cells, and bistratified ganglion cells (Schubert et al., 2005 a,b; Völgyi et al., 2005 b). Deletion of Cx45 in neurons has been shown to disrupt coupling between ACs and ON cone bipolar cells (Maxeiner et al., 2005). Mice lacking Cx36 and/or Cx45 in neurons showed that the number of ACs coupling to ganglion cells was significantly reduced when compared to control. This finding led researchers to suggest that both Cx36 and Cx45 participate in coupling between ganglion cells and displaced ACs (Schubert et al., 2005; Pan et al., 2010; Pang et al., 2013). Therefore, Cx36 and Cx45 serve as prime candidates for potentially coupling ipRGCs to displaced ACs. Using transgenic mouse lines in which Cx36 or Cx45 are specifically eliminated in ipRGCs provides a new approach to understanding more about these photoreceptors, the cells coupled to them and discovering how coupling between ipRGCs and ACs contribute to image-forming vision. In this study, we have

directly examined the tracer patterns of M1-M6 type ipRGCs in the mouse retina by intracellular injections of the gap-junction permeable tracer, Neurobiotin (NB).

4.3 Results

As explained in Chapter 2, we crossed *Opn4*$^{Cre/+}$*: GFP* mice with Cx36 and Cx45 flox lines to created mice in which GFP-labeled ipRGCs lacked either the Cx36 gene or the Cx45 gene. The flox lines activate GFP expression in cells where the desired connexin gene has been excised. The ipRGC-Cx36$^{-/-}$ mice were created successfully within a year, but despite our repeated attempts, we never observed robust GFP expression in ipRGCs in the ipRGC-Cx45$^{-/-}$ mice and therefore, Cx45 was not successfully knocked out in all ipRGCs (Figure 4.1). Thus, we performed the NB injection experiments only on the ipRGC-Cx36$^{-/-}$ retinas. In the control and ipRGC-Cx36$^{-/-}$ mouse lines, we injected GFP-positive cells in the GCL with Neurobiotin (a gap-junction permeable tracer) and Lucifer Yellow (LY), which does not cross most gap junctions—to analyze the morphology and tracer-coupling patterns of ipRGCs. LY allowed validation of successful cell impalement prior to injection with Neurobiotin. Prior to injection of NB+LY solution, GFP signal could normally be seen in the soma of ipRGCs, and occasionally, a few dendrites and axons of GFP expressing ipRGCs could also be detected.

ipRGC types

All six types of ipRGCs, M1-M6, were well-filled with Neurobiotin and analyzed after fixed retinas had been incubated with Streptavidin 568 (Figure 4.3, a-b). M1-M6 ipRGC types were identified based on their dendritic morphologies and stratification levels in the inner plexiform

layer (IPL), and identification was consistent with previously reported findings (Hattar et al., 2006; Schmidt et al., 2008; Schmidth and Kofuji et al., 2009; Muller et al., 2010; Reifler et al., 2015; Quattrochi et al., 2019). All M1 ipRGCs had dendrites that stratified in the OFF sublamina layer of IPL. M2, M4 and M5 ipRGCs had dendrites that stratified in the ON sublamina layer of the IPL; while M3 and M6 ipRGCs' dendrites stratified in both ON and OFF sublamina layers of the IPL.

Cells coupled to ipRGCs

Using a ganglion cell marker, RBPMS, we found that ipRGC-coupled cells were not ganglion cells (19/19 retinas, 100%) but instead were positive for GABA (7/19 retinas, 36%), an amacrine cell marker (Figure 4.2). Therefore, cells coupled to ipRGCs are ACs. Muller et al found that M1-M3 type ipRGCs are tracer- coupled to amacrine cells. Our research examined a larger population of ipRGCs (n> 50 retinas) and supports the findings that M1-M3 type ipRGCs are coupled to displaced ACs (Muller et al., 2010). We also examined whether the remaining ipRGC types, M4-M6, are tracer- coupled to amacrine cells and whether the absence of Cx36 altered the number of coupled cells. On average, retinas with normal Cx36 levels, types M2, M4 and M3 are coupled to more ACs that M1, M5 and M6 types (Figure 4.3, a,b). This could be due to the fact that the dendritic arbors for M2 and M4 type ipRGCs are greater than that of M1 (Muller et al., 2010).

Connexin 36 mediates coupling between ipRGCs and displaced ACs.

The average number of ACs that couple with ipRGCs was reduced in ipRGC-Cx36$^{-/-}$ mice (Figure 4.3 b,c). On average, each type of ipRGC in the ipRGC-Cx36$^{-/-}$ were coupled to fewer

cells when compared to control. Specifically in the ipRGC-Cx36$^{-/-}$, M2 and M4 type ipRGCs showed significant reduction ($p<0.05$) in the average number of coupled cells (>2 and >1, respectively) compared to M2 and M4 type ipRGCs in the control line (>4 and >7, respectively) (Figure 4.3, c).

Identify which types of amacrine cells are coupled to ipRGCs.

Since ipRGC gap-junction coupled cells are amacrine cells and not ganglion cells (e.g. ipRGCs or conventional ganglion cells), it was worth exploring which types of amacrine cells are electrically coupled to ipRGCs. There are over 30 different types of amacrine cells in the mouse retina and it is well known that amacrine cells contain various neuromodulators and neurotransmitters that can modulate the responses of retinal neurons. After immunostaining for several neuromodulators, all of the ipRGC-coupled amacrine cells were immunonegative for choline-acetyl-transferase (ChAT) and vasoactive intestinal polypeptide (VIP) (Figure 4.4, a). In contrast, ipRGC-coupled amacrine cells were immunopositive for serotonin (5-HT) (26%), brain nitric oxide synthase (bNOS) (100%), neuropeptide Y (NPY) (14%) (Figure 4.4, b-c) or neuronal nitric oxide synthase (nNOS) (4.5%) (Figure 3.3). See table below for detailed analysis of neuromodulators identified (Table 4.1).

Amacrine cells identified by neuromodulator content	Number of ipRGC-coupled ACs immunopositive	Total number of ipRGC-coupled ACs	Type of ipRGC coupled to identified ACs
5-HT	4	15	M2, M3 and M4
bNOS	2	2	M3
NPY	3	21	M3 and M4
nNOS	6	132	N/A*

Table 4.1: Biochemical characterization of ipRGC-coupled ACs. Detailed analysis of number biochemical characterization of ipRGC-coupled amacrine cells. *nNOS positive cells were identified in *rd1*$^{-/-}$*rd12*$^{-/-}$ retinas and were not injected with Neurobiotin.

Soma diameter comparison of ipRGC-coupled cells

Not only do amacrine cells differ in their neuromodulator or neurotransmitter content but also vary in morphology and size. Previous work from Pang at el (Pang et al., 2013) reported that mouse amacrine cells' soma diameters ranged between ~5-15µm. We decided to group the coupled cells into 3 bins (5µm, 10µm or15µm) based on soma diameter in microns (µm). If the soma diameter of a coupled cell ranged from 2.5µm -7.5µm, it was placed in the 5µm bin. If the soma diameter ranged from 7.6µm-12.5µm, it was placed in the 10µm bin. Finally, if the soma diameter ranged from 12.6µm-17.5µm, it was placed in the largest bin, 15µm.

In the control retinas, the majority of coupled cells in M1-M6 type ipRGCs were placed in the 10µm bin category (Figure 4.5, a-b). A small portion of coupled cells fell in the 5µm bin category within each ipRGC type and less than 45% of coupled cells within each type were placed in the largest bin category, 15µm (Figure 4.5, a-b). However, in the ipRGC-Cx36$^{-/-}$ line, the number of coupled cells identified in M2, M3, M5 and M6 type ipRGCs were placed in either the 10µm (M2: n=8, M3: n=39 and M5: n=1) or the 5µm (M2: n=1, M3: n=7 and M6: n=1) bins while no coupled cells fell within the largest bin category, 15µm except for M3-type coupled cells (n=3) (Figure 4.5, b). Within these ipRGC types, it seems as though Cx36 is needed to couple large displaced amacrine cells, that is whose soma diameter is greater or equal to 12.6µm, to ipRGCs.

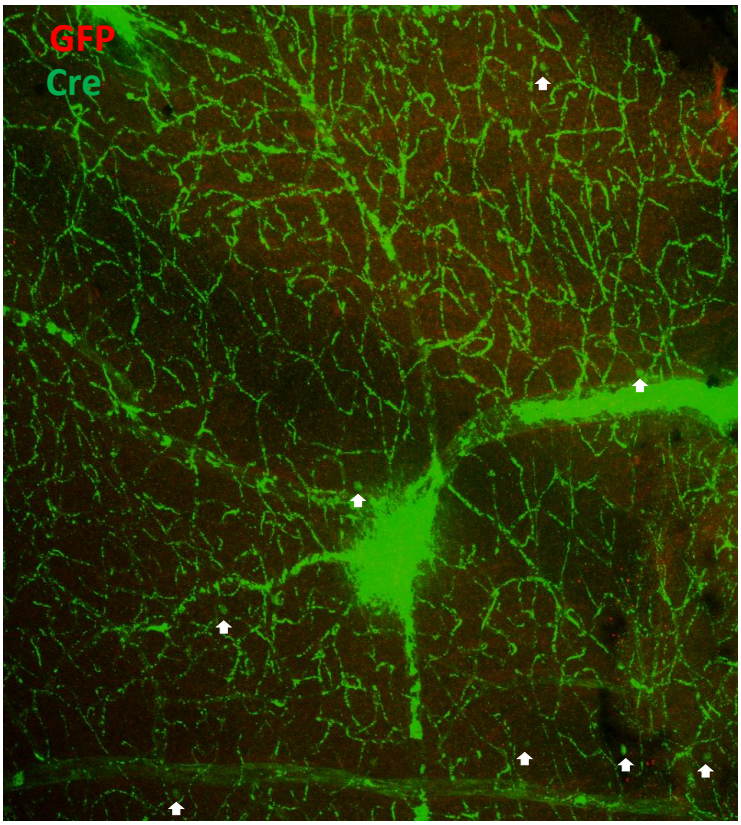

Figure 4.1: Lack of localization between GFP and Cre cells in the ipRGC-Cx45$^{-/-}$ mouse line. White arrow heads represent Cre positive cells, ipRGCs. Cre (FITC) and GFP (Cy3).

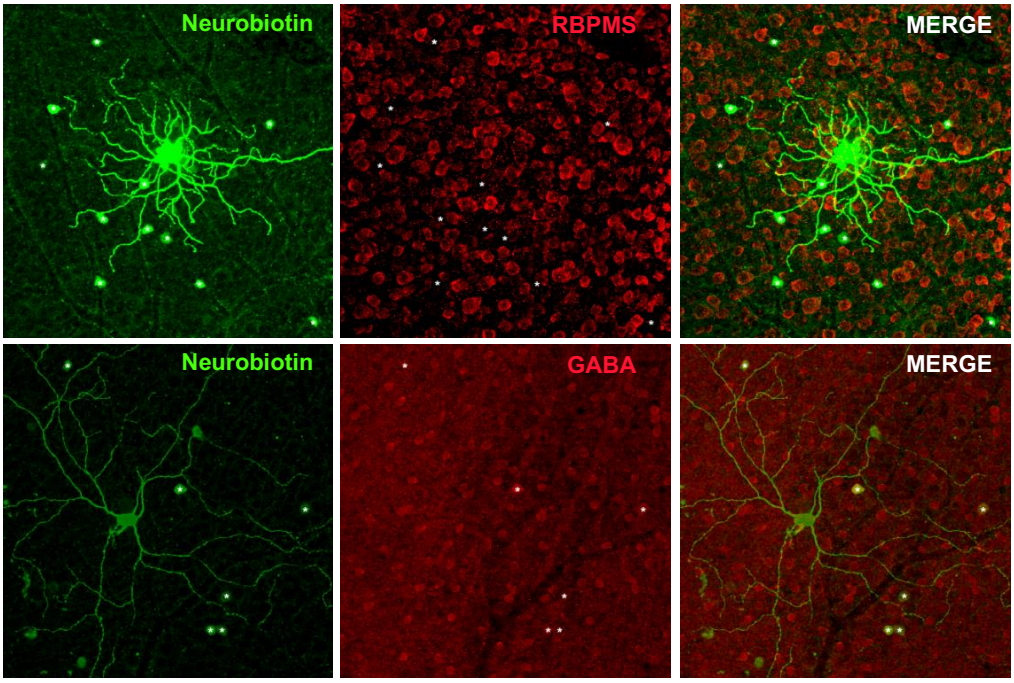

Figure 4.2: ipRGC-coupled cells are amacrine cells. ipRGCs were injected with Neurobiotin (*left column:* M4 type ipRGC (top) and M3 type ipRGC (bottom)) and retinas were stained with anti-rabbit RBPMS, a ganglion cell marker (*top middle column*) or anti-rabbit GABA, an amacrine cell marker (*bottom middle column*). ipRGC-coupled cells were negative for RBPMS (100%) and positive for GABA (36%), indicating ipRGCs are tracer coupled to amacrine cells.

A.

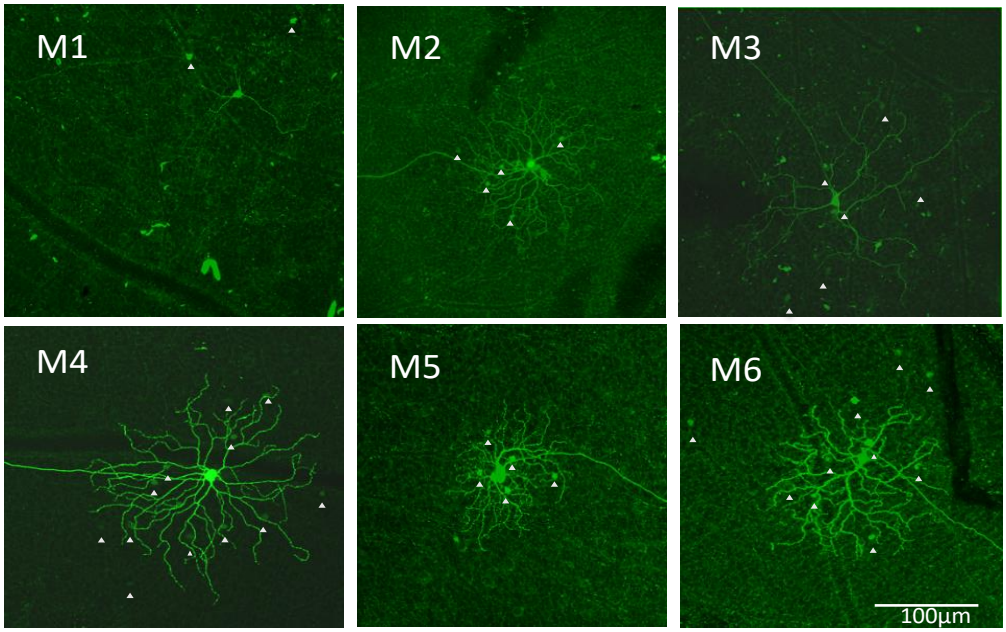

B.

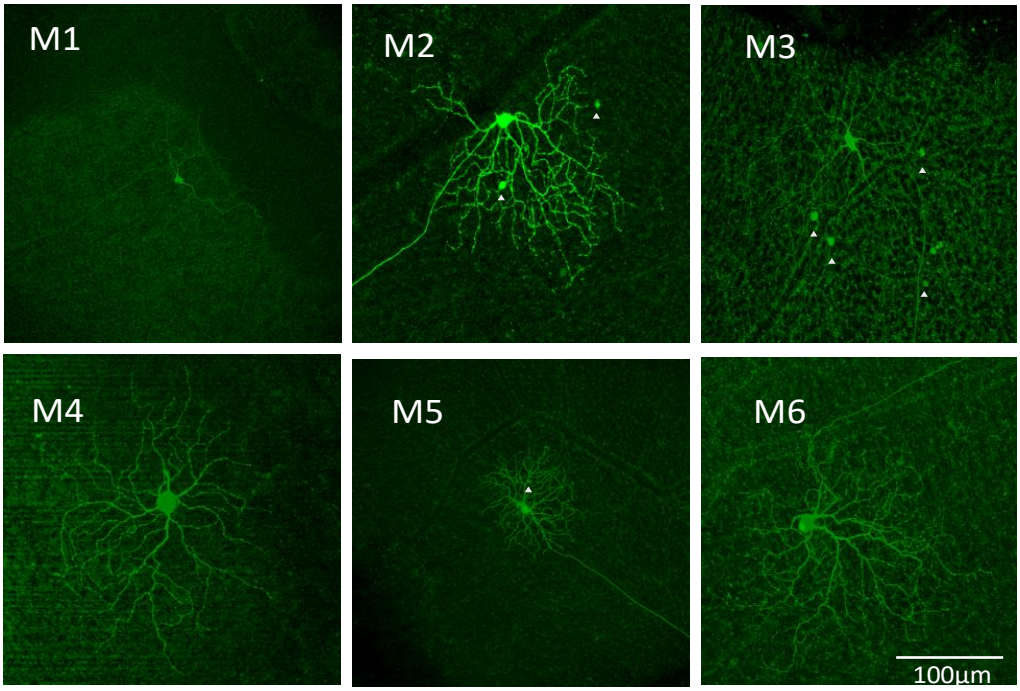

C.

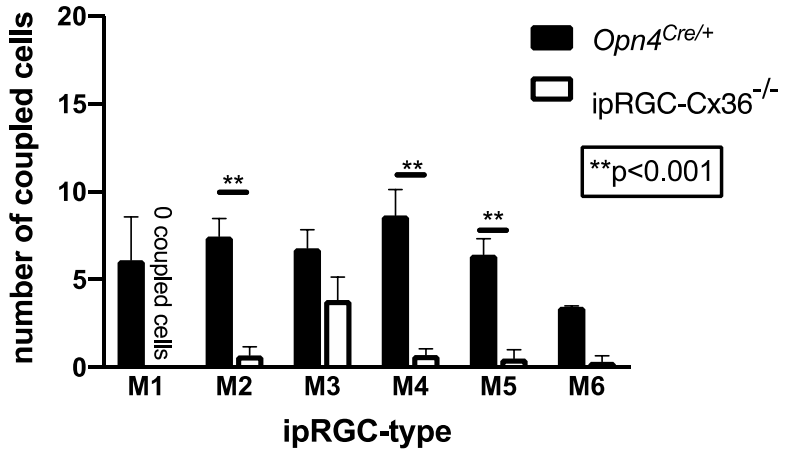

Figure 4.3: ipRGC-AC coupling is dependent on connexin 36 for most ipRGC types. Confocal images of Neurobiotin injected ipRGCs (M1-M6) in *A)* control retinas (*Opn4*$^{Cre/+}$), and *B)* ipRGC-Cx36$^{-/-}$ retinas. The ipRGC-coupled ACs are denoted by arrow heads. *C)* Histogram indicting the mean (± SEM) number of coupled amacrine cells to each ipRGC type in both control and ipRGC-Cx36$^{-/-}$ mouse lines. Both M2 and M4 type ipRGC is significantly different in the ipRGC-Cx36$^{-/-}$ line when compared to *Opn4*$^{Cre/+}$ (p=.01). The number of cells analyzed: M1 cells (n=9), M2 (n=31), M3 (n=33), M4 (n=24), M5 (n=19) and M6 (n=20) in *Opn4*$^{Cre/+}$ retinas. The number of cells analyzed in ipRGC-Cx36$^{-/-}$ retinas: M1 cells (n=5), M2 (n=13), M3 (n=13), M4 (n=17), M5 (n=4) and M6 (n=3). Scale bar = 100µm

A.

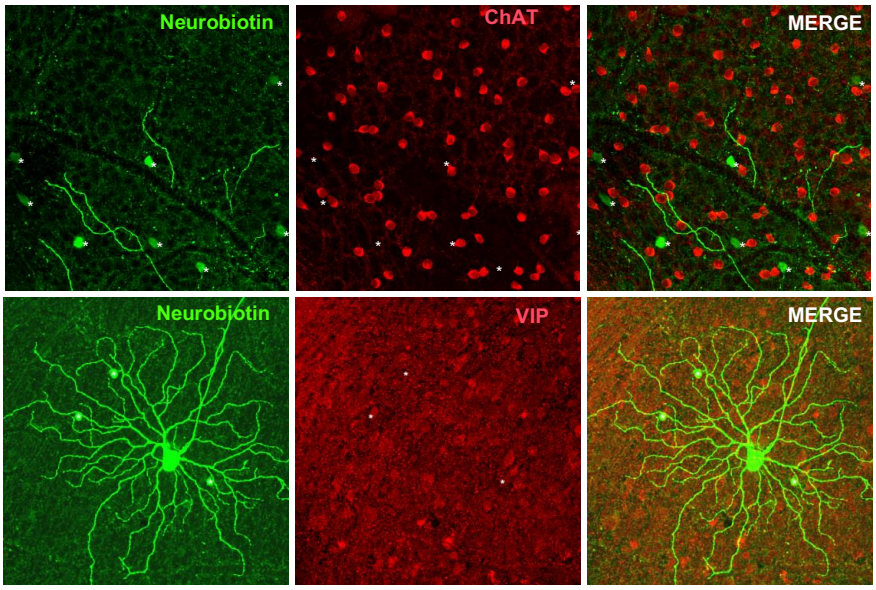
Neurobiotin
ChAT
MERGE
Neurobiotin
VIP
MERGE

B.

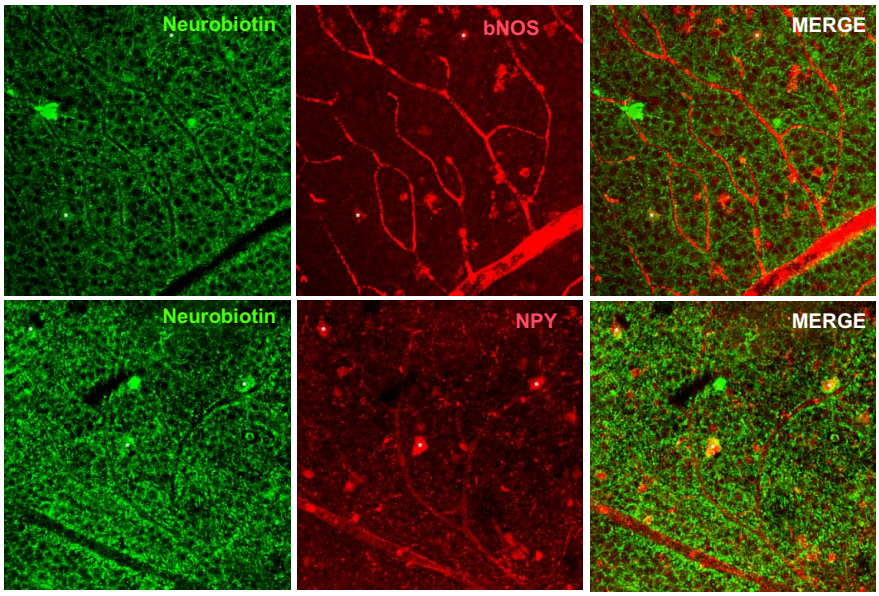
Neurobiotin
bNOS
MERGE
Neurobiotin
NPY
MERGE

C.

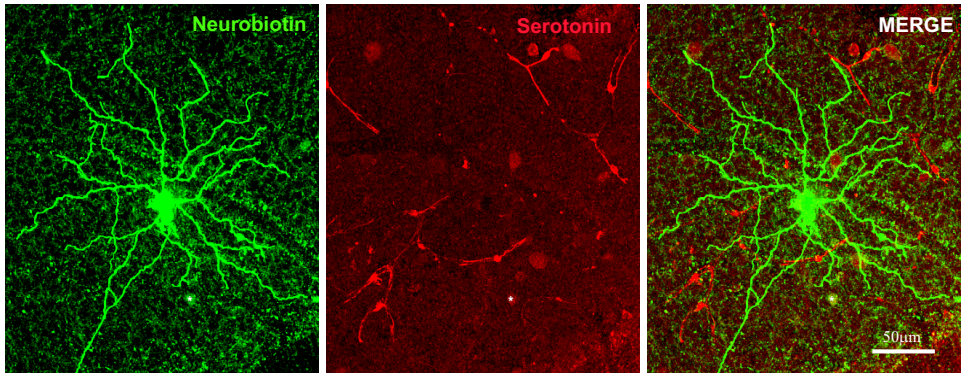

Figure 4.4: Biochemical characterization of ipRGC-coupled amacrine cells. ipRGC-coupled amacrine cells are *A)* immunonegative for ChAT and VIP, while immunopositive for *B)* bNOS, NPY and *C)* serotonin (5-HT). Immunopositive cells are denoted by asterisks. Scale bar =50µm.

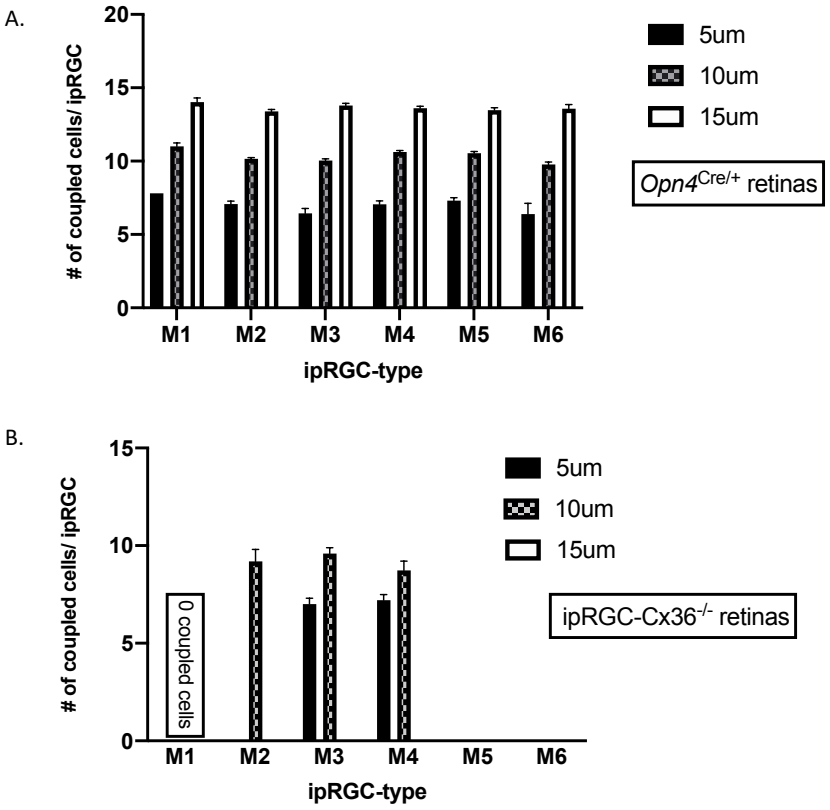

Figure 4.5: Soma diameter distribution of ipRGC coupled amacrine cells by ipRGC type. *A)* wild-type retinas (*Opn4*$^{Cre/+}$) and *B)* ipRGC-Cx36$^{-/-}$ retinas. The coupled cells were grouped into 3 bins based on soma diameter in microns (μm): 5μm, 10μm or 15μm.

4.4 Discussion

In mice older than two months of age, Muller et al. reported that on average, 5.3 amacrine cells on average were coupled to M1 type ipRGCs, while with M2 and M3- type ipRGCs are tracer-coupled to more amacrine cells, 10.3 and 10 respectively. Additionally, they reported that ipRGC-coupled amacrine cells were located in the ganglion cell layer of the retina (GCL) as opposed to their more commonly identified location, the inner nuclear layer (INL), and therefore, such amacrine cells have been termed displaced amacrine cells (dACs). While, these findings shed light on the potential interactions of ipRGCs via electrical coupling, two major caveats existed. Firstly, the sample size for M3, was extremely low (n=3), and only one cell showed tracer coupling. Secondly, since their report, additional ipRGC types have been discovered since their report. As a result, they were not able to provide an analysis of these newly identified types, M4-M6. Our study further extended the previously reported results and showed that M1-M6 type ipRGCs are tracer-coupled to multiple amacrine cells. In our study the counting of ipRGC-coupled amacrine cells was dependent on NB diffusing into the coupled cells. Some cells showed bright NB staining while others showed faint and weak staining. Regardless of whether the NB staining in the coupled cells was strong or weak, signals were clearly distinguishable from the background staining. Additionally, the total number of ipRGC-coupled amacrine cells varied between ipRGCs of the same type. For example, one M2 would be coupled to 5 amacrine cells while another would be coupled to roughly 10 amacrine cells. How can we be sure that we detected all the amacrine cells coupled to each ipRGC type? Schubert et al examined GC-AC coupling via tracer injections. They reported that the number of amacrine cells coupled to GCs was maximized when injections lasted 30-minutes as opposed to 15-minutes or 20-minutes. However, when we tried various injection durations, specifically 15, 20 or 30-minutes, we did not notice a difference in the average

number of coupled amacrine cells. Our 15-minute injection duration was longer than Muller et al, who reported their findings injecting NB into ipRGCs for 3 minutes.

Both ganglion cells and amacrine cells are classified into more than 20 morphological types within the mammalian retina and thus, it was worth exploring the types of amacrine cells coupled to each type of ipRGC. Amacrine cells are commonly identified immunologically by antibodies against either their neurotransmitter or neuromodulator content. Some commonly identified contents in amacrine cells are: GABA, glycine, ChAT and neuronal or brain nitric oxide synthase (nNOS or bNOS) and the population percentage of these types of amacrine cells have been explored (Kolb, 1997; Vaney et al., 1998; MacNeil et al., 1999; Muller et al., 2007; Pang et al., 2013; Jason et al., 2018). In the mammalian retina, homologous coupling is often present between ganglion cells (Volgyi et al., 2009) and GABA amacrine cells (Vaney et al., 2004) and even between nNOS ACs (Jason et al., 2018). However, we never observed ipRGCs coupling with other retinal ganglion cells (RGCs).

We noticed a shift in the types of amacrine cells coupled to each ipRGC types in the ipRGC-Cx36$^{-/-}$ mouse line. It was previously reported that amacrine cells coupled to RGCs varied in soma sizes ranging from large to small in the control line (Pang et al., 2013). Our control data is consistent with the findings from Pang et al; amacrine cells coupled to ganglion cells varied in soma sizes (Pang et al., 2013). Although there was a significant and clear reduction in the average number of coupled cells per ipRGC type in the ipRGC-Cx36$^{-/-}$ mouse line when compared to wild-type control, the fact remains that eliminating these connexins did not completely abolish ipRGC-AC coupling. Initially, we entertained the possibility that Cx45 also mediates coupling between ipRGCs and amacrine cells. Indeed, both Cx36 and Cx45 are found within the IPL, with Cx45-expressing neurons coupling via Cx45 and Cx36-

expressing neurons coupling via Cx36 (Li et al., 2008). We attempted to assess the contribution Cx45 has in ipRGC-AC coupling but after multiple attempts, we failed to successfully eliminate Cx45 in all ipRGCs and therefore, we were unable to probe for a contribution of Cx45 in ipRGC-A coupling using NB injection. However, this does not mean that Cx45 does not contribute to coupling and future exploration should still be considered. Another potential candidate was Cx30.2. It was previously found that connexin 30.2 is expressed in six types of ganglion cells (one type ON-OFF, three types of OFF, and two types of ON ganglion cells) and therefore might contribute to coupling ganglion cells to amacrine cells (Muller et al, 2010a; Meyer et al., 2016). Specifically, it was found that RG_{A1} cells, which resemble the M4-type ipRGC, were heterologously coupled to multiple displaced ACs and the extent of this coupling is mediated by protein kinase C (Muller et al., 2010b). However, to date there are no reports that have identified the contribution of Cx30.2 specifically in ipRGC-AC coupling via tracer injections and therefore, Cx30.2 is still a potential candidate coupling ipRGCs to displaced amacrine cells.

In conclusion, using tracer injections, we directly examined the tracer patterns of M1-M6 type ipRGCs in the mouse retina and concluded that all ipRGCs are coupled to displaced amacrine cells via gap junctions. Furthermore, there was a significant reduction in the average number of coupled cells in the ipRGC-$Cx36^{-/-}$ mouse line when compared to control. Our findings clearly demonstrate a role for Cx36 in ipRGC-AC coupling but functionally, what is Cx36's role in ipRGC-AC coupling? One major hypothesis that can be driven from the findings presented here and from previous reports is that in response to light, ipRGCs depolarize and current flows from them into the coupled amacrine cells, which in turn triggers the release of neurotransmitters and neurotransmitters from various populations of amacrine cells as evident by the differences in ipRGC-coupled amacrine cell soma diameters. When

ipRGCs lack Cx36, the number of coupled amacrine cells significantly decreased and that variety of amacrine cells shifted. One speculation for the shift in variety of amacrine cells is that there was less exchange of ions and metabolites between ipRGCs and these coupled amacrine cells. A recent study examined the exchange of small molecules, specifically GABA, between amacrine cells and ganglion cells (Marc et al., 2018). As a result of using small molecule markers and connectomics, they concluded that some ganglion cells which formed gap junctions with GABA-positive amacrine cells contained GABA. This result provided a potential mechanism in which an excited ganglion cell could inhibit, nearby ganglion cells indirectly. Although, in our case, we did not find that ipRGCs were tracer-coupled to GABA-positive amacrine cells, it is possible that the identified ipRGC tracer-coupled amacrine cells, 5-TH, bNOS, nNOS and NPY, may diffuse their molecular contents to ipRGCs, since gap junctional coupling is bidirectional (Rozental et al., 2001; Sohl et al., 2004; Sosinsky et al., 2005). Therefore, it is highly possible that the shift in the variety of coupled amacrine cells observed in the ipRGC-Cx36$^{-/-}$ line could be due to the fact that this exchange of ions between ipRGCs and larger soma amacrine cells has been abolished.

The easiest way to determine the behavioral role of ipRGC-AC coupling is to compare the optokinetic reflexes of ipRGC-Cx36$^{-/-}$ mice and control mice. However, a few (5-10%) rods and cones express Cre in the melanopsin-Cre mouse line (Ecker et al., 2010), and so in the ipRGC-Cx36$^{-/-}$ mice, Cx36 is presumably knocked out not only in ipRGCs but also in some rods and cones. This is expected to attenuate rod-cone coupling to some degree (Bolte et al., 2016), potentially affecting visual behavior including the optokinetic reflex. For this reason, ipRGC-Cx36$^{-/-}$ mice cannot be used to study the behavioral role of ipRGC-AC coupling specifically, and we decided not to examine the optokinetic reflex of these mice.

We detected 5-HT, NPY, bNOS or nNOS in a small subset of ipRGC-coupled ACs. For decades, it has been known that 5-HT is synthesized and released in the retina by only amacrine cells. Both bipolar cells and ganglion cells have 5-HT receptors needed to uptake 5-HT release from amacrine cells and 5-HT receptor-mediated regulation has been shown to play a role in visual acuity and retinal neuroprotection (George et al., 2005; Tullis et al., 2015 Li et al., 2016). Similarly, work uncovering the role NPY in retinal development has led to discovering its contribution to modulation and development in retinal synaptogenesis (Ferriero and Sagar, 1989; Hustler and Chalpua, 1995) and many neuroprotective effects (Alvaro et al., 2009; Santos-Carvalho et al., 2013b). So far, the last neuromodulator identified, nitric oxide (NO), is commonly recognized as a neuronal messenger molecule and is produced in many areas of the body and contains various isoforms (Riveros-Moreno et al., 1993). Specifically, in the retina, NO is involved in the control of retinal blood flow under basal conditions (Deussen et al., 1993), photoreceptor light transduction and synaptic input (Kurenny et al., 1994). In cats, the effects of NO synthase had a profound inhibition on the electroretinogram where both a-wave and b-wave responses decreased significantly in response to 10-second white light flashes (Ostwald et al., 1995; Goldstein et al., 1995). As mentioned, we identified two NO isoforms coupled to ipRGCs: bNOS and nNOS. nNOS has been found to modulate neurogenesis and memory (Zhou and Zhu, 2009) while bNOS is active within the developing LGN and has expanded the role of NO during early postnatal development (Mccauley et al., 2003).

In this chapter, we only identified a few amacrine cells tracer-coupled to ipRGCs. The fact remains that the retina contains dozens of amacrine cells and it is very likely that many more are

tracer-coupled to ipRGCs. Therefore, it is worth exploring additional neuromodulators tracer-coupled to ipRGCs to better understand the role they play in the retina. Understanding the types of ACs coupled to ipRGCs could uncover their contribution in modulating the light responses of other retinal neurons such as bipolar cells and conventional ganglion cells and ultimately its effects on image-forming vision.

Chapter 5 Glutamatergic Input to ipRGCs Modulates ipRGC-AC Coupling

5.1 Abstract

One of the main purposes of the retina is to quickly encode environmental stimuli so the brain can further process information in our visual scene. Glutamate is the primary excitatory neurotransmitter in the vertebrate retina and serves a key role in retinal synaptic circuitry. The release of glutamate is dependent on membrane polarization and stimulus intensity, which ultimately impacts the signaling cascade to inner retinal neurons. Therefore, an understanding of its function and contribution to retinal neurobiology is critical. While previous work has explored how glutamate regulates gap-junctional coupling between the AII amacrine cell network via non-synaptic N-methyl-D-aspartate (NMDA) receptors (Kothman et al., 2012), work uncovering how it modulates cell-to-cell coupling patterns between ipRGCs and displaced amacrine cells has not been undertaken. Here, we report that the absence of NMDA glutamate receptors on ipRGCs weakens coupling patterns with displaced amacrine cells. The implication is that bipolar cell mediated glutamatergic activation of NMDA receptors in ipRGCs promotes ipRGC-AC coupling, either acutely or developmentally or both.

5.2 Introduction

Photoreceptors are responsible for converting photons into electrical signals and transmitting visual signals to bipolar cells which in turn mediate signal transfer to inner retinal neurons. Cone photoreceptors release glutamate onto bipolar cells, which express either inhibitory (sign-inverting) metabotropic or excitatory (sign-preserving) ionotropic receptors and thus initiate parallel OFF and ON pathways (Nakajima et al., 1993; Muller, 2008). Bipolar cells then release glutamate onto ganglion cells which collectively express multiple receptor types (Marc et al., 1990; Davanger et al., 1994; Taschenberger and Grantyn, 1995; Jojich and Pourcho, 1996). Once released from presynaptic terminals, glutamate diffuses across the synaptic cleft and then binds to its receptors (GluRs, AMPA/kainate or NMDA) on the dendrites of post-synaptic cells (Conn and Pin, 1997; Ozawa et al., 1998).

N-methyl-D-aspartate (NMDA) receptors are a type of ionotropic glutamate receptors permeable to Na^+, K^+, and Ca^{2+}, and once activated produce long-lasting electrical changes within post-synaptic neurons (Yang, 2004). Ganglion cells express NMDA receptors as evident by immunocytochemical and in situ hybridization studies (Hughes et al., 1992; Muller et al., 1992b; Vandenbranden et al., 2000) and are present on the dendrites of most ganglion cell types (Grunert et al., 2002). It has been proposed that NMDA receptors on ganglion cells play a vital role in synaptic transmission. In primate ganglion cells, extensive research has revealed that blocking NMDA receptors gives rise to transient light responses (Cohen and Miller, 1994), NMDA receptor mediated photoresponses have relatively fast kinetics (Stafford et al., 2014; Crook et al., 2014), and both NMDARs and AMPARs complement each other to generate excitatory synaptic currents producing voltage-independent amplitudes (Diamond and

Copenhagen, 1993; 1995). It has also been demonstrated that in a cell-type specific manner, NMDA receptors contribute to visual contrast coding Manookin et al., 2011).

In total, seven genes encode the NMDA receptor subunits: four *GRIN2* genes encode GluN2A-D, one *GRIN1* gene encodes GluN1, and two *GRIN3* genes encode GluN3A-B (Traynelis et al., 2010). The GluN1 and GluN2 subunits have an affinity towards glycine and glutamate, respectively (Hansen et al., 2013). GluN1 is widely expressed in all central neurons and is an essential subunit in all-functional NMDA receptors; therefore, inactivation of this subunit abolishes NMDA receptor function.

We, therefore wanted to take this knowledge and create a mouse line in which all ipRGCs lack *GRIN1,* ipRGC-*nr1*$^{-/-}$, and examine the effect on ipRGC-AC coupling patterns. To achieve this end, an intracellular tracer was injected into fluorescently labeled ipRGCs and allowed to diffuse into the coupled cells. After antibody characterization, the ipRGC type and the coupled cells were visualized, and analyses were made.

5.3 Results

We injected Neurobiotin into GFP-labeled ipRGCs and counted the number of coupled amacrine cells in mice in which NR1 was knocked out only in ipRGCs and in control mice (Figure 5.1 and Table 5.1).

A.

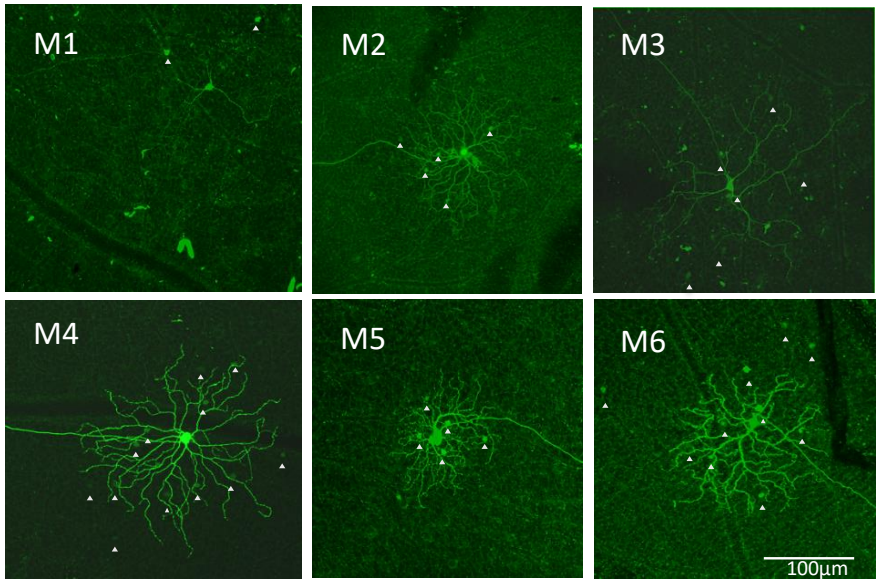

B.

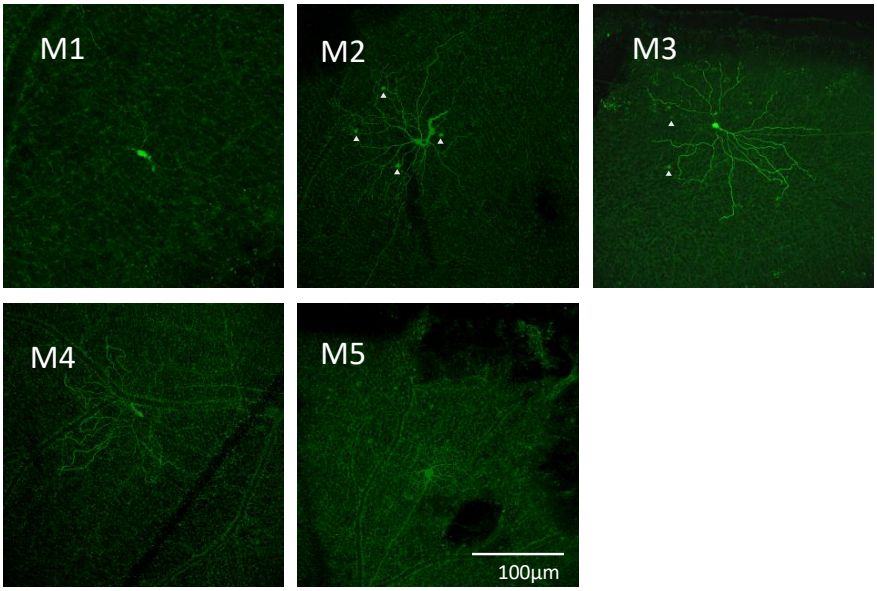

Figure 5.1: Inactivation of NDMA receptors on ipRGCs disrupts coupling between ipRGCs and displaced amacrine cells. Confocal images of Neurobiotin injected ipRGCs (M1-M6) in *A)* wild-type retinas (*Opn4*$^{Cre/+}$), and (M1-M5) in *B)* ipRGC-*nr1*$^{-/-}$ retinas. No data from M6 ipRGCs was gathered in the ipRGC-*nr1*$^{-/-}$ retinas. The coupled displaced amacrine cells are denoted by arrow heads. Scale bar = 100µm

	Opn4$^{Cre/+}$				ipRGC-*nr1*$^{-/-}$		
ipRGC type	**Number of cells studied**	**# of ipRGCs with coupled amacrine cells**	**Average number of coupled amacrine cells (Mean +/- SEM)**		**Number of cells studied**	**# of ipRGCs with coupled amacrine cells**	**Average number of coupled amacrine cells (Mean +/- SEM)**
M1	19	9	6.11 (2.468)		2	1	0.50 (0.5)
M2	39	31	7.45 (1.023)		6	3	1.50 (0.806)
M3	45	34	6.78 (1.045)		7	3	1.28 (0.606)
M4*	30	24	8.66 (1.454)		6	1	0.666 (0.666)
M5	26	19	6.42 (0.901)		2	0	0.000 (0)
M6	24	20	3.45 (0.638)		n/a	n/a	n/a

Table 5.1: Comparison of ipRGC-coupled ACs between control and ipRGC-*nr1*$^{-/-}$. The average number of coupled cells in the M4 type ipRGC is significantly different in the ipRGC-NR1$^{-/-}$ line when compared to *Opn4*$^{Cre/+}$ (*p=.05). In the ipRGC-*nr1*$^{-/-}$ mouse line, there is no data available for the M6 type ipRGC.

Knowing that amacrine cells make up a diverse population of neurons in the retina, we wanted to make a crude analysis on the size of the amacrine cells coupled to ipRGCs. The soma diameters of the coupled cells were compared in each type. The coupled amacrine cells were grouped into 3 bins (5 microns, 10 microns, and 15 microns) based on soma diameter in microns (μm)- similar to the analysis made in Chapter 4. If the soma diameter of a coupled cell ranged from 2.5μm - 7.5μm, it was placed in the 5μm bin category. If the soma diameter ranged from 7.6μm-12.5μm, it was placed in the 10μm bin category. Finally, if the soma diameter ranged from 12.6μm-17.5μm, it was placed in the largest bin category, 15μm.

In the control line, majority of the tracer-coupled amacrine cells within each ipRGC type were placed in either the 10μm or 15μm bin categories (Figure 5.2, a). However, a noticeable

phenotype was observed in the ipRGC-*nr1*$^{-/-}$ line. Amacrine cells tracer-coupled to M1-type ipRGCs were placed in the smallest bin size, 5µm (n=1) (Figure 5.2, b). There were no other coupled cells from the remaining ipRGC types that were coupled to cells small enough to be included in this bin size. Both M2 and M4 type ipRGCs had amacrine cells placed in the 10µm and 15µm bin (n=1; n=2) with more than 75% of coupled cells falling in the 10µm bin category (n=8) and 50% of coupled cells in the 10µm bin category (n=2), respectively (Figure 5.2, b). Amacrine cells tracer-coupled to M3-type ipRGCs all fell within the 10µm bin category (n=9). Finally, M5-type ipRGCs were not coupled to amacrine cells and we did not generate data from M6 ipRGCs.

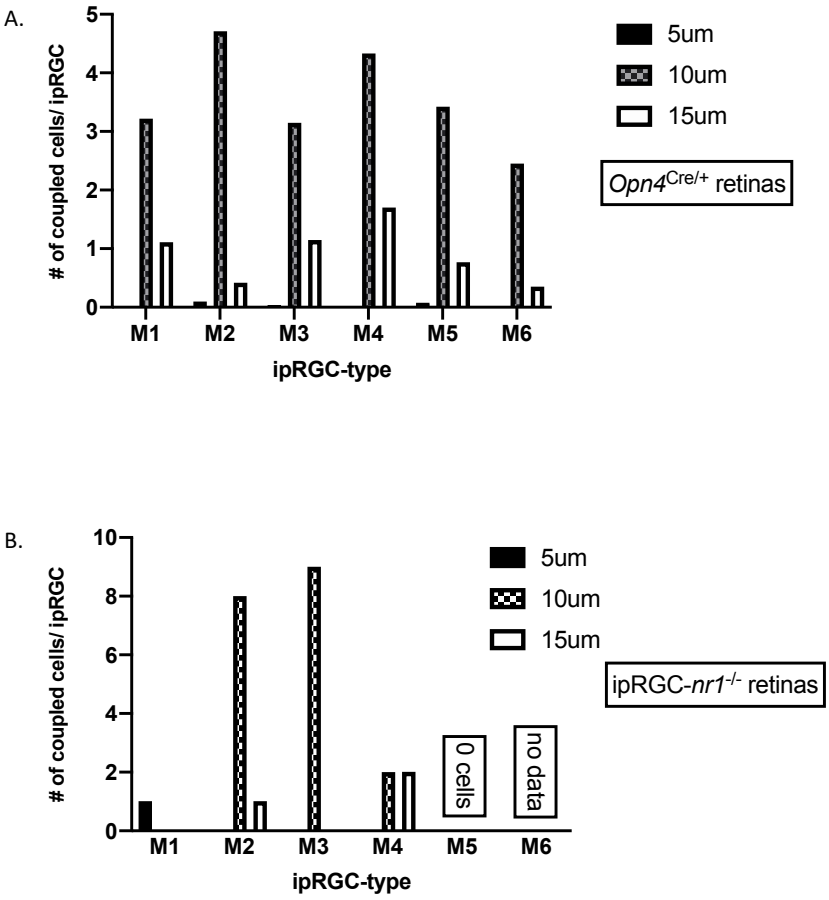

Figure 5.2: Soma diameter distribution of ipRGC-coupled amacrine cells by ipRGC type. *A) Opn4*$^{Cre/+}$retinas (control), and *B)* ipRGC-*nr1*$^{-/-}$ retinas. The coupled cells were grouped into 3 bins based on soma diameter in microns (μm): 5μm, 10μm or15μm. As explained in Table 5.1, the M5 type ipRGC in the NR1$^{-/-}$ did not have any coupled cells and there was no data for M6 type ipRGC in the ipRGC-*nr1*$^{-/-}$ retinas.

5.4 Discussion

The absence of NR1 in all ipRGCs impacted the coupling patterns between ipRGCs and displaced amacrine cells as shown by the reduction of average coupled cells in 5 out of 6 ipRGC types. Furthermore, it seems as if the presence of NMDA receptors strengthens coupling between amacrine cells with a diameter between 7.6μm-12.5μm. Since NR1 was knocked out unconditionally in ipRGCs, the observed reduction in ipRGC-AC coupling could reflect developmental alteration as well as acute neuromodulatory effects. We decided not to examine acute effects by bath-applying NMDA receptor antagonists because this would affect NMDA signaling throughout the retina, rather than in ipRGCs specifically. While we previously had success blocking NMDA receptors intracellularly by including MK801 in the whole-cell recording micropipette (Zhao et al., 2017), the feasibility of this approach has not been verified for sharp electrodes.

In the absence of NMDA receptors, M1 type ipRGCs were coupled exclusively to amacrine cells falling in the smallest bin category, 5μm and M2 and M3 type ipRGCs were coupled primarily to cells in the 10μm bin diameter category (Figure 5.2, b). Interestingly enough in the ipRGC-*nr1*$^{-/-}$ line, the distribution has shifted greatly with less than 25% of soma diameters larger than 12.5μm- specifically in M1, M2, M3 and M5 type ipRGCs. In addition, in the ipRGC-*nr1*$^{-/-}$ line, amacrine cells coupled to M4 type ipRGCs no longer fell within the smallest soma diameter category but were equally distributed between the largest bin, 15μm, and the medium bin, 10μm.

Without functional NMDA receptors, the majority of ipRGCs couple to smaller amacrine cells which could highlight the importance of NMDA coupling between ipRGCs and displaced amacrine cells as well as the various types of amacrine cells gap-junction coupled to ipRGCs.

Previous work has demonstrated dopaminergic modulation of ipRGCs (Sakamoto et al., 2005; Van Hook et al., 2012), however, dopaminergic modulation of ipRGC-AC coupling has not been examined specifically. It has been proposed that dopamine and NMDA receptor activation modulate gap junctions in the IPL in opposite ways. Coupling within neuronal networks is often regulated by multiple factors such as background illumination in which many sensory systems must adapt to these conditions. It is through this adaptation that modulation of coupling strength is often assessed (Xin and Bloomfield, 1999; Bloomfield and Volgyi, 2004). For example, electrical coupling is strengthened once NMDA receptors are activated (Kothmann et al., 2012; Turecek et al., 2014) while dopamine stimulates dephosphorylation of Cx36 mediated AII amacrine cell coupling (Kothmann et al., 2009). Additionally, the activation of dopamine D4 receptors was found to subdue coupling and PKA activity during the daytime (Li et al., 2013). In contrast, Li et al. also found that at night, adenosine A2a receptors increase PKA activity at night and therefore enhanced coupling patterns (Li et al., 2013). Furthermore, it was concluded that the circadian clocks regulate rod-cone coupling as coupling patterns are reduced during the subjective day and by adaptation to bright light (Ribelayga et al., 2008).

Chapter 6 Rods, Cones and Melanopsin on Image-forming Vision

The majority of this chapter has been published: Schroeder MM, * Harrison KR,* Jaeckel ER, Berger HN, Zhao X, Flannery MP, St. Pierre EC, Pategi N, Jachimska A, Chervenak AP, Wong KY (*Co-first authors): The roles of rods, cones and melanopsin in photoresponses of M4 intrinsically photosensitive retinal ganglion cell (ipRGC) and optokinetic visual behavior. *Frontiers in Cellular Neuroscience:* 2018.

The text below was written specifically for this thesis and was not copy-and-pasted from the published paper.

6.1 Abstract

The visual system not only enables us to discern form, color and motion in our world ("image-forming vision") but also drives various subconscious physiological responses to light such as pupillary light reflex (PLR), suppression of melatonin secretion and circadian photoentrainment ("non image-forming vision"). Originally, rods and cones were believed to mediate image-forming vision, while non image-forming vision was assumed to be driven primarily by intrinsically photosensitive retinal ganglion cells (ipRGCs), which use the photopigment melanopsin to sense light. However, recent research has yielded increasing evidence that M4-type ipRGCs innervate image-forming visual nuclei and contribute to image-forming vision

(Estevez et al., 2012; Zhao et al., 2014; Schmidt et al., 2014), yet the functional roles of these three photoreceptive systems (rods, cones and melanopsin) remain poorly understood. To fill in this knowledge gap, four mouse strains' behavioral responses were compared: 1) wild-type mice (WT); 2) *Gnat1*$^{-/-}$ mice with non-photosensitive rods; 3) *Gnat2*^{cpfl3} mice with non-photosensitive cones; and 4) melanopsin-knockout mice (*Opn4*$^{-/-}$) in which the intrinsic photosensitivity of ipRGCs is abolished. To test image-forming visual responses, the OptoMotry apparatus (CerebralMechanics, Inc.) was used to measure optokinetic responses to rotating striped stimuli at various drift speeds, contrast levels and spatial frequencies. The results suggest that while all three photoreceptive systems contribute to contrast sensitivity, primarily cones determine spatial acuity while both rods and cones are important for tracking slow-moving stripes. In conclusion, rods, cones and ipRGCs contribute differentially to image-forming vision.

6.2 Introduction

The initial stages of visual processing originate in the retina. Rod and cone photoreceptors convert light into electric signals. Information is then received by horizontal cells, bipolar cells, amacrine cells and ultimately ganglion cells, which are responsible for sending information to the brain for further visual processing. Up until 2002, researchers in the field presumed that rod and cones were the only photoreceptors in the retina. A small population of RGCs uses the photopigment melanopsin to respond directly to light and thus serve as photoreceptors in the retina (Provencio et al., 1998; Berson et al., 2002; Hattar et al., 2002; Graham et al., 2008; Xue et al., 2011). Additionally, all ipRGCs receive rod and cone- mediated depolarizing light responses (Dacey et al., 2005; Wong et al., 2007; Schmidt and Kofuji, 2010, 2011; Weng et al., 2013; Zhao

et al., 2014). Though originally it was thought that ipRGC axons only project to non-image-forming brain nuclei to drive subconscious physiological responses to light such as circadian photoentrainment, pupillary light reflex and the suppression of melatonin secretion (Berson et al., 2003; Hattar et al., 2006) we now know that they also innervate image-forming visual centers and mediate contrast detection, pattern vision and brightness discrimination (Ecker et al., 2010; Brown et al., 2012; Schmidt et al., 2014). Additionally, M1-M4 type ipRGCs project to the superior colliculus (SC), a brain area known to detect novel objects in the visual scene (Zhao et al., 2014).

While the roles of rod/cone inputs to ipRGCs are well understood, e.g. increase an ipRGC's light response (Dacey et al., 2005; Wong et al., 2007), generate receptive field properties such as center/surround antagonism (Estevez et al., 2012; Zhao et al., 2014), speed alteration (Zhao et al., 2014) and color opponency (Dacey et al., 2005; Stabio et al., 2017), how rod input and cone input differentially contribute functionally with ipRGCs remain poorly understood. Previously, members of the Wong lab performed whole-cell recordings on M4-type ipRGCs in mice lacking either cones, rods or melanopsin and found that all three components contribute to response sustainedness. Furthermore, it was shown that the initial peak in a light-step response originates from rod and cone inputs. Finally, it was shown that post-stimulus persistence of the response comes mainly from the rod input, not melanopsin, whereas stimulus tracking utilizes rod input, cone input, or both, depending on light frequency and intensity. Together, these results prompted us to examine the roles of the three photoreceptive systems in spatial visual behavior by studying how selectively disrupting each system affects optokinetic tracking behavior.

6.3 Results

The elimination of rod, cone or melanopsin showed defects in visual behavior. In the first parameter tested, spatial acuity, eliminating cone and rod input had the greatest significant reduction, which resulted in acuities that were lower than both wild-type and melanopsin knockout. Eliminating melanopsin did not affect the spatial acuity of the animals tested (Figure 6.1, a). Drift speed (deg/sec (s)) was the second parameter tested. Four speeds were examined: 8 deg/s, 12 deg/s, 16 deg/s, and 20 deg/s. At each speed tested, excluding cone function showed significant reduction in spatial acuity when compared to control littermates (Figure 6.1, b). Rods showed to be important for tracking slower speeds: 8 deg/s and 12 deg/s while in contrast, melanopsin is important only for tracking the slowest speed tested, 8 deg/s (Figure 6.1, b).

Finally, four spatial frequency values were tested during the contrast sensitivity parameter: 0.042 cyc/deg, 0.092 cyc/deg, 0.192 cyc/deg, 0.272 cyc/deg, all at the same speed 12 deg/s. By comparable amounts, contrast sensitivity was significantly reduced in the melanopsin-knockout, rod-functionless and cone-functionless mice at the third highest spatial frequency value tested (Figure 6.1, c). Both cone and rod functionless mice showed a significant reduction at the highest spatial frequency (Figure 6.1, c).

A.

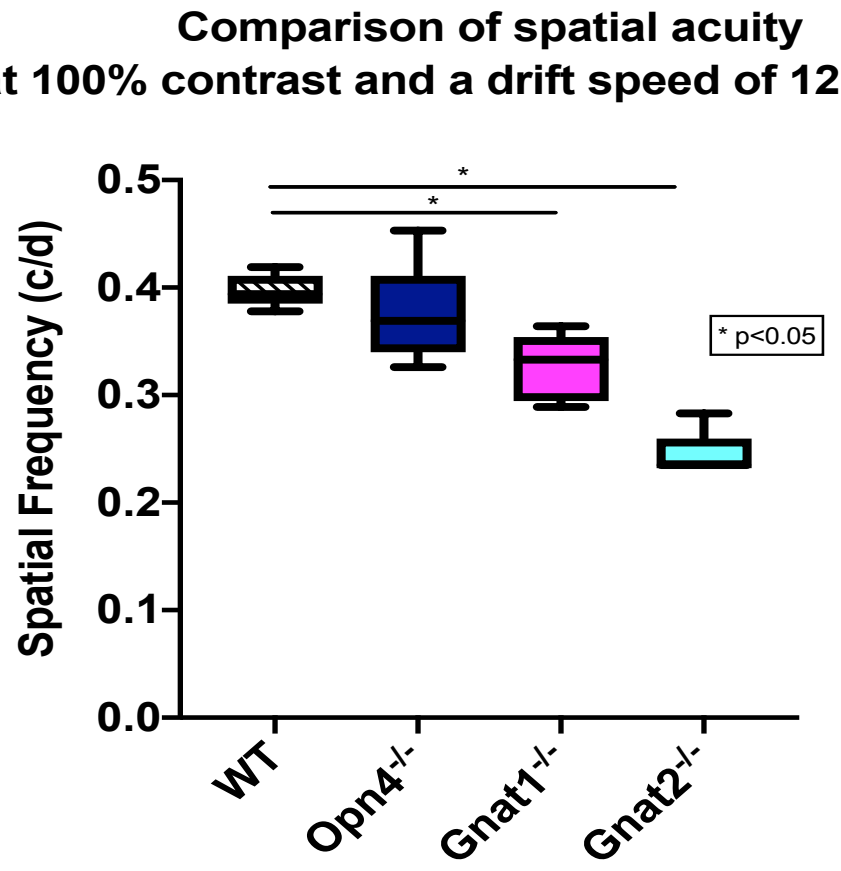
Comparison of spatial acuity
(at 100% contrast and a drift speed of 12 deg s-1)
Spatial Frequency (c/d)
0.5
0.4
0.3
0.2
0.1
0.0
*
*
* p<0.05
WT
Opn4+/-
Gnat1-/-
Gnat2-/-

B.

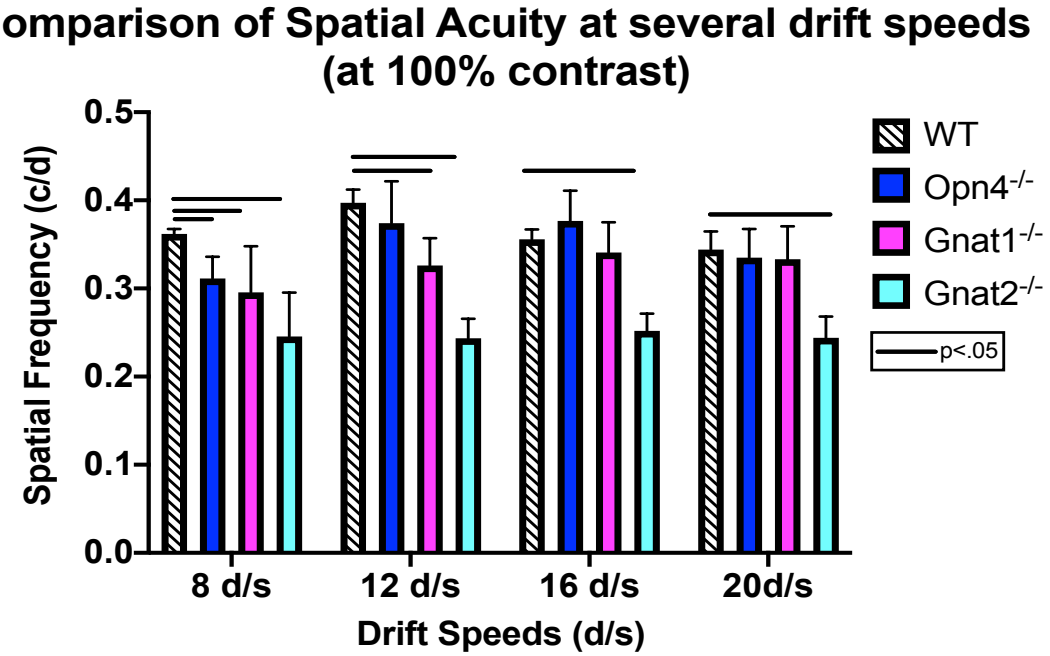
Comparison of Spatial Acuity at several drift speeds
(at 100% contrast)
Spatial Frequency (c/d)
0.5
0.4
0.3
0.2
0.1
0.0
8 d/s
12 d/s
16 d/s
20d/s
Drift Speeds (d/s)
WT
Opn4-/-
Gnat1-/-
Gnat2-/-
p<.05

C.

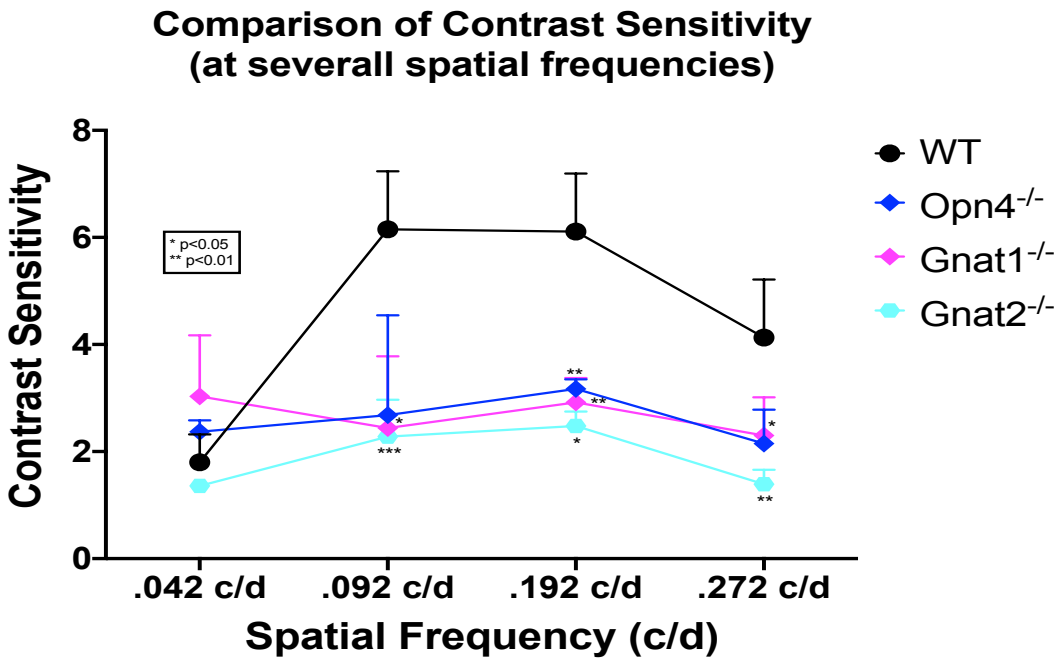

Figure 6.1: Contribution of photoreceptors on visual behavior. *A)* Acuity was assessed using sine wave gratings with 100% contrast at drift speed 12 deg/sec. *B)* at four different drift speeds. *C)* Contrast sensitivity was assessed using sine wave gratings with four different spatial frequencies, all drifting at 12 deg/sec. In all three experiments all mice were male, 4-6 months old, and n=5 mice per genotype for each testing condition.

6.4 Discussion

Schmidt et al. found a role for melanopsin in contrast sensitivity (Schmidt et al., 2014) by using an optokinetic tracking assay identical to ours. While our results showed that for some spatial frequencies, melanopsin's role in contrast sensitivity may be as equally important as rods' and cones' we, in contrast to their results found spatial acuity to be determined by rods and cones alone. Our findings are consistent with the melanopsin-only (lacking functional rod and cone input) mice lacking the ability to optokinetically track a stimulus (Ecker et al., 2010). For acuity, cones were found to be more important than rods as silencing cones reduced acuity by the greatest amount at all drift speeds. Since the stimulus intensity measured at the cornea is in the photopic range where rods are saturated, this result was expected (Dacey et al., 2005). In spite of this, rods did contribute to acuity at one drift speed, which may seem surprising given the photopic testing conditions, but recent work showed that rods gradually regain photosensitivity after initial saturation by daylight conditions (Tikidji-Hamburyan et al., 2017).

By eliminating each photoreceptive system, we have found that all three photoreceptive systems (rods, cones, and melanopsin) play an important role in contrast sensitivity while visual acuity is primarily dependent on cones and to lesser extent rods. Additionally, we show that rods, cones and melanopsin are necessary for tracking slow speeds while rods in contrast are solely necessary for tracking speeds faster than 8d/s.

Chapter 7 Contributions to Field

This dissertation helped uncover many of the unsolved questions within the field while gaining more insight into importance of ipRGC intraretinal signaling. We found that ipRGC-coupled amacrine cells are distributed differentially across the mammalian retina specifically, there are more ipRGC-coupled amacrine cells located in the dorsal, nasal and temporal regions of the retina compared to the ventral region of the mammalian retina. Through intracellular injections, we showed that M1-M3 type ipRGCs are gap-junction coupled to amacrine cells, results similar to Muller et al. (Muller et al., 2010). Furthermore, we also found that amacrine cells are also gap-junction coupled to three additional types of ipRGCs, M4-M6- a discovery that has not been shown previously in the field. Pang et al's work highlighted that amacrine cells coupled to ganglion cells vary in soma size (Pang et al., 2013) and using this same approach, we concluded that all ipRGCs are coupled to mainly medium size amacrine cells with a few coupling to small and large amacrine cells and identified Cx36 to be essential for coupling a few amacrine cells to ipRGCs.

Not only was it important to expand the body of work from Muller et al, but we then wanted to begin identifying the types of amacrine cells coupled to ipRGCs. While there are over 20 different types of amacrine cells identified in the mammalian retina, we identified four types of amacrine cells that couple to ipRGCs: nNOS, bNOS, NPY and serotonin (5-HT). However, amacrine cells containing ChAT and VIP were not gap-junction coupled to ipRGCs. By now, it

is well known that amacrine cells contain various neuromodulators and neurotransmitters that are released into the retina and potentially modulate the light responses of other retinal neurons. Previous work from Wong et al. found that ipRGCs express functional glutamate receptors and that these functional roles have yet to be explored. Therefore, to further understand the effect of synaptic input on ipRGC-AC coupling, we generated a mouse line in which NMDA glutamate receptors were inactive on all ipRGCs and assessed the coupling patterns between ipRGCs and amacrine cells through intracellular injections. We concluded that knocking out NMDA receptors in ipRGCs significantly reduced the number of coupled amacrine cells and ultimately weakened coupling specifically in M2, M3, M4 and M5 type ipRGCs when compared to control littermates. As a result, ipRGC-AC coupling is modulated by synaptic input.

Last but not least, since the discovery of ipRGCs and their role in non-image-forming vision, researchers have begun discovering their unique role in image-forming vision. However, understanding the individual contribution ipRGCs, rods and cones contribute to image-forming vision remain unexplored. Through optokinetic tracking, we showed that spatial acuity is determined primary by cones, rods are important for tracking slow-moving stripes whereas cones are necessary for tracking all speeds tested and all three photoreceptive systems (rods, cones and melanopsin) contribute to contrast sensitivity (Schroeder et al., 2018).

Chapter 8 Future Directions

What additional types of amacrine cells are coupled to ipRGCs?

Pang et al surveyed amacrine cells coupled to ganglion cells and concluded that amacrine cells not only varied in neuromodulator content but also in size as evident by measuring the soma diameter of the coupled amacrine cells (Pang et al., 2013). Similarly, we also were able to conclude that amacrine cells coupled to ipRGCs varied in sizes ranging from small (2.5μm - 7.5μm) to large (12.6μm -17.5μm). Additionally, we successfully identified a few types of amacrine cells gap-junction coupled to ipRGCs specifically amacrine cells containing bNOS, NPY, 5-HT or nNOS. While our work uncovered that 4 types of amacrine cells are gap-junction coupled to ipRGCs, we know that there are at least 20 additional types of amacrine cells to explore (Massland., 2001). Using immunocytochemistry, it was found that displaced amacrine cells, which are amacrine cells located in the ganglion cell layer of the retina were positive for markers labeling CCKS, catecholamine, substance P and somatostatin (Cervia et al., 2008; Casini et al., 2005; Cristiani et al., 2002; Mitrofanis et al., 1988; Versaux-Botteri et al., 1986). It is possible that one or a few of these amacrine cells are coupled to ipRGCs; therefore, it is worth exploring whether amacrine cells containing CCKS, catecholamine, substance P, and somatostatin are gap-junction coupled to ipRGCs.

Are specific types of ipRGC-coupled amacrine cells distributed differently across the retina?

To better understand the role ipRGC-coupled amacrine cells contribute to retinal physiology, knowing where these cells are located would help researchers fill in this knowledge gap. Based on the analysis made, we've concluded that ipRGC-coupled amacrine cells are distributed differentially across the retina. Specifically, in the dorsal, ventral and nasal regions of the retina there are more ipRGC-coupled amacrine cells than ipRGCs, whereas there are more ipRGCs than ipRGC-coupled amacrine cells in the temporal region of the retina. We did not however examine the types of ipRGC-coupled amacrine cells located in these retinal regions. For example, are there more 5-HT- positive amacrine cells located in the dorsal region of the retina compared to the other 3 regions? Using immunocytochemistry to stain for various neuromodulators in the dorsal, temporal, nasal and ventral regions of the retina would allow us to examine if specific types of amacrine cells are located predominately in one retinal region compared others. This in-depth analyses would then allow us to begin examining the functional roles these amacrine cells play and their importance of receiving input from ipRGCs.

What other connexin is involved in coupling ipRGCs to amacrine cells?

When we deleted Cx36 from all ipRGCs, we found that ipRGC-AC coupling was significantly reduced compared to control littermates; nonetheless, coupling was not completely abolished. Therefore, it is likely that there are additional connexins playing a role in coupling ipRGCs to amacrine cells. As discussed in Chapter 4's Discussion, a potential connexin candidate to explore is Cx30.2. By injecting Neurobiotin into GFP-expressing ipRGCs lacking Cx30.2 and assessing the coupling patterns between all types of ipRGCs and coupled amacrine cells would lead us to

conclude whether Cx30.2 contributes to ipRGC-AC coupling and to what extent. If coupling persists, then it is also possible that Cx36 and Cx30.2 form heteromeric connexons meaning one cell contributes two different types of connexins to create a connexon (see Figure 1.8). Additionally, it is still worth exploring the possibility that Cx45 contributes to ipRGC-AC coupling despite our failed attempts.

To what extent does modulation of ipRGC-to-amacrine cell coupling effect the light responses of other retinal neurons?

If deleting NMDA receptors from ipRGCs decreased the average number of ipRGC-coupled amacrine cells when compared to control littermates, what additional effect does this have on other retinal neurons in response to light? Presumably, the release of neurotransmitters and neuromodulators from amacrine cells may modulate the light responses of bipolar cells and photoreceptors, for example. Using the electroretinogram, a field potential that reflects the light responses of rods and cones, ON bipolar cells, and amacrine cells we could examine the a-wave, which depicts the responses from rod and cone photoreceptors, and the b-wave, which examines the responses of bipolar cells to assess the light responses of other retinal neurons in mice lacking functional NMDA receptors and compare traces with control littermates. Work from Hankins and Lucas found that photostimulation of melanopsin modulates the kinetics of ON bipolar cell light responses and therefore, intraretinal signaling by ipRGCs has been shown to modulate the human ERG (Hankins and Lucas, 2003). Despite this, the synaptic mechanisms remain unknown.

Bibliography

1. N. M. Alam, C. M. Altimus, R. M. Douglas, S. Hattar, G. T. Prusky, Photoreceptor regulation of spatial visual behavior. *Invest Ophthalmol Vis Sci* **56**, 1842-1849 (2015).
2. A. E. Allen *et al.*, Melanopsin-driven light adaptation in mouse vision. *Curr Biol* **24**, 2481-2490 (2014).
3. A. R. Alvaro, J. Rosmaninho-Salgado, A. F. Ambrosio, C. Cavadas, Neuropeptide Y inhibits [Ca2+]i changes in rat retinal neurons through NPY Y1, Y4, and Y5 receptors. *J Neurochem* **109**, 1508-1515 (2009).
4. A. R. Barnard, S. Hattar, M. W. Hankins, R. J. Lucas, Melanopsin regulates visual processing in the mouse retina. *Curr Biol* **16**, 389-395 (2006).
5. D. M. Berson, A. M. Castrucci, I. Provencio, Morphology and mosaics of melanopsin-expressing retinal ganglion cell types in mice. *J Comp Neurol* **518**, 2405-2422 (2010).
6. D. M. Berson, F. A. Dunn, M. Takao, Phototransduction by retinal ganglion cells that set the circadian clock. *Science* **295**, 1070-1073 (2002).
7. A. G. Blankenship *et al.*, The role of neuronal connexins 36 and 45 in shaping spontaneous firing patterns in the developing retina. *J Neurosci* **31**, 9998-10008 (2011).
8. J. Blom, T. Giove, M. Deshpande, W. D. Eldred, Characterization of nitric oxide signaling pathways in the mouse retina. *J Comp Neurol* **520**, 4204-4217 (2012).
9. S. A. Bloomfield, B. Volgyi, The diverse functional roles and regulation of neuronal gap junctions in the retina. *Nat Rev Neurosci* **10**, 495-506 (2009).
10. S. A. Bloomfield, D. Xin, A comparison of receptive-field and tracer-coupling size of amacrine and ganglion cells in the rabbit retina. *Vis Neurosci* **14**, 1153-1165 (1997).
11. D. S. G. Bredt, C.E.; Hwang, P.M.; Fotuhi, M.; Dawson, T.M.; Snyder, S.H, Nitric Oxide Snythase Protein and mRNA Are Discretely Localized in Neuronal Populations of the Mammalian CNS Together with NADPH Diaphorase. *Neuron* **7**, 615-624 (1991).
12. T. M. Brown *et al.*, Melanopsin contributions to irradiance coding in the thalamo-cortical visual system. *PLoS Biol* **8**, e1000558 (2010).
13. L. Cao, W. D. Eldred, Subcellular localization of neuronal nitric oxide synthase in turtle retina: electron immunocytochemistry. *Vis Neurosci* **18**, 949-960 (2001).
14. C. A. Czeisler *et al.*, Suppression of melatonin secretion in some blind patients by exposure to bright light. *N Engl J Med* **332**, 6-11 (1995).

15. M. R. Deans, B. Volgyi, D. A. Goodenough, S. A. Bloomfield, D. L. Paul, Connexin36 is essential for transmission of rod-mediated visual signals in the mammalian retina. *Neuron* **36**, 703-712 (2002).
16. K. Dedek *et al.*, Localization of heterotypic gap junctions composed of connexin45 and connexin36 in the rod pathway of the mouse retina. *Eur J Neurosci* **24**, 1675-1686 (2006).
17. A. Delwig *et al.*, Retinofugal Projections from Melanopsin-Expressing Retinal Ganglion Cells Revealed by Intraocular Injections of Cre-Dependent Virus. *PLoS One* **11**, e0149501 (2016).
18. R. M. Douglas *et al.*, Independent visual threshold measurements in the two eyes of freely moving rats and mice using a virtual-reality optokinetic system. *Vis Neurosci* **22**, 677-684 (2005).
19. U. C. Drager, J. F. Olsen, Ganglion cell distribution in the retina of the mouse. *Invest Ophthalmol Vis Sci* **20**, 285-293 (1981).
20. J. L. Ecker *et al.*, Melanopsin-expressing retinal ganglion-cell photoreceptors: cellular diversity and role in pattern vision. *Neuron* **67**, 49-60 (2010).
21. W. D. Eldred, T. A. Blute, Imaging of nitric oxide in the retina. *Vision Res* **45**, 3469-3486 (2005).
22. E. M. Ellis, G. Gauvain, B. Sivyer, G. J. Murphy, Shared and distinct retinal input to the mouse superior colliculus and dorsal lateral geniculate nucleus. *J Neurophysiol* **116**, 602-610 (2016).
23. M. E. Estevez *et al.*, Form and function of the M4 cell, an intrinsically photosensitive retinal ganglion cell type contributing to geniculocortical vision. *J Neurosci* **32**, 13608-13620 (2012).
24. D. M. Ferriero, S. M. Sagar, Development of neuropeptide Y-immunoreactive neurons in the rat retina. *Brain Res Dev Brain Res* **48**, 19-26 (1989).
25. U. S. Forsterman, W.C, Nitric oxide synthases: regulation and function. *European Heart Journal* **33**, 829-837 (2012).
26. R. G. Foster *et al.*, Circadian photoreception in the retinally degenerate mouse (rd/rd). *J Comp Physiol A* **169**, 39-50 (1991).
27. M. S. Freedman *et al.*, Regulation of mammalian circadian behavior by non-rod, non-cone, ocular photoreceptors. *Science* **284**, 502-504 (1999).
28. G. J. Gage, D. R. Kipke, W. Shain, Whole animal perfusion fixation for rodents. *J Vis Exp*, (2012).
29. J. M. Garcia-Fernandez, A. J. Jimenez, R. G. Foster, The persistence of cone photoreceptors within the dorsal retina of aged retinally degenerate mice (rd/rd): implications for circadian organization. *Neurosci Lett* **187**, 33-36 (1995).
30. L. Gianfranceschi, A. Fiorentini, L. Maffei, Behavioural visual acuity of wild type and bcl2 transgenic mouse. *Vision Res* **39**, 569-574 (1999).
31. I. M. O. Goldstein, P.; Roth, S., Nitric Oxide- A Review of its Role in Retinal Function and Disease. *Vision Res* **36**, 2979-2994 (1995).
32. D. M. W. Graham, K.Y, Melanopsin-expressing, Intrinsically Photosensitive Retinal Ganglion Cells (ipRGCs). *Webvision*, (2008).

33. F. A. Hafezi, M.; Grimm, C.; Wenzel, A.; Munz, K.; Sturmer, J.; Farber, D.B.; Reme, C, Retinal Degeneration in the rd Mouse in the Absence of cfos. *Investigative Ophthalmology & Visual Science* **39**, 2239-2244 (1998).
34. M. W. Hankins, R. J. Lucas, The primary visual pathway in humans is regulated according to long-term light exposure through the action of a nonclassical photopigment. *Curr Biol* **12**, 191-198 (2002).
35. J. V. Hannibal, N.; Card, P.; Fahrenkrug, J., Light-dependent induction of cFos during subjective day and night in PACAP-containing ganglion cells of the retinohypothalamic tract. *Journal of Biological Rhythms* **16**, 457-470 (2001).
36. K. B. Hansen *et al.*, Structure, function, and allosteric modulation of NMDA receptors. *The Journal of General Physiology* **150**, 1081-1105 (2018).
37. G. E. Hardingham, H. Bading, Synaptic versus extrasynaptic NMDA receptor signalling: implications for neurodegenerative disorders. *Nat Rev Neurosci* **11**, 682-696 (2010).
38. M. Hatori *et al.*, Inducible ablation of melanopsin-expressing retinal ganglion cells reveals their central role in non-image forming visual responses. *PLoS One* **3**, e2451 (2008).
39. S. Hattar *et al.*, Central projections of melanopsin-expressing retinal ganglion cells in the mouse. *J Comp Neurol* **497**, 326-349 (2006).
40. S. Hattar, H. W. Liao, M. Takao, D. M. Berson, K. W. Yau, Melanopsin-containing retinal ganglion cells: architecture, projections, and intrinsic photosensitivity. *Science* **295**, 1065-1070 (2002).
41. B. Hoffpauir, E. McMains, E. Gleason, Nitric oxide transiently converts synaptic inhibition to excitation in retinal amacrine cells. *J Neurophysiol* **95**, 2866-2877 (2006).
42. J. J. L. Huerta, M.M.; Cernuda-Cernuda, R.; Garcia-Fernandez, J.M., Fos expression in the retina of rd:rd mice during the light/dark cycles. *Elsevier-Neuroscience Letters* **232**, 143-146 (1997).
43. S. Hughes *et al.*, Characterisation of light responses in the retina of mice lacking principle components of rod, cone and melanopsin phototransduction signalling pathways. *Sci Rep* **6**, 28086 (2016).
44. S. Hughes, T. S. Watson, R. G. Foster, S. N. Peirson, M. W. Hankins, Nonuniform distribution and spectral tuning of photosensitive retinal ganglion cells of the mouse retina. *Curr Biol* **23**, 1696-1701 (2013).
45. J. J. Hutsler, L. M. Chalupa, Development of neuropeptide Y immunoreactive amacrine and ganglion cells in the pre- and postnatal cat retina. *J Comp Neurol* **361**, 152-164 (1995).
46. J. Jacoby, A. Nath, Z. F. Jessen, G. W. Schwartz, A Self-Regulating Gap Junction Network of Amacrine Cells Controls Nitric Oxide Release in the Retina. *Neuron* **100**, 1149-1162 e1145 (2018).
47. V. Jain, E. Ravindran, N. K. Dhingra, Differential expression of Brn3 transcription factors in intrinsically photosensitive retinal ganglion cells in mouse. *J Comp Neurol* **520**, 742-755 (2012).

48. C. J. Jeon, E. Strettoi, R. H. Masland, The major cell populations of the mouse retina. *J Neurosci* **18**, 8936-8946 (1998).
49. A. M. Kaufman *et al.*, Opposing Roles of Synaptic and Extrasynaptic NMDA Receptor Signaling in Cocultured Striatal and Cortical Neurons. *Journal of Neuroscience* **32**, 3992-4003 (2012).
50. A. Kawasaki, R. H. Kardon, Intrinsically photosensitive retinal ganglion cells. *J Neuroophthalmol* **27**, 195-204 (2007).
51. R. B. King, A. Deussen, G. M. Raymond, J. B. Bassingthwaighte, A vascular transport operator. *Am J Physiol* **265**, H2196-2208 (1993).
52. J. S. Koistinaho, S., Light-induced c-fos expression in amacrine cells in the rabbit retina *Molecular Brain Research* 53-63 (1995).
53. W. W. Kothmann, S. C. Massey, J. O'Brien, Dopamine-stimulated dephosphorylation of connexin 36 mediates AII amacrine cell uncoupling. *J Neurosci* **29**, 14903-14911 (2009).
54. W. W. Kothmann *et al.*, Nonsynaptic NMDA receptors mediate activity-dependent plasticity of gap junctional coupling in the AII amacrine cell network. *J Neurosci* **32**, 6747-6759 (2012).
55. V. Krishnan, E. Gleason, Nitric oxide releases Cl(-) from acidic organelles in retinal amacrine cells. *Front Cell Neurosci* **9**, 213 (2015).
56. O. Kruger *et al.*, Defective vascular development in connexin 45-deficient mice. *Development* **127**, 4179-4193 (2000).
57. D. E. Kurenny, L. L. Moroz, R. W. Turner, K. A. Sharkey, S. Barnes, Modulation of ion channels in rod photoreceptors by nitric oxide. *Neuron* **13**, 315-324 (1994).
58. E. J. Lee *et al.*, The immunocytochemical localization of connexin 36 at rod and cone gap junctions in the guinea pig retina. *Eur J Neurosci* **18**, 2925-2934 (2003).
59. H. Li *et al.*, Adenosine and dopamine receptors coregulate photoreceptor coupling via gap junction phosphorylation in mouse retina. *J Neurosci* **33**, 3135-3150 (2013).
60. L. L. Liu, N. J. Spix, D. Q. Zhang, NMDA Receptors Contribute to Retrograde Synaptic Transmission from Ganglion Cell Photoreceptors to Dopaminergic Amacrine Cells. *Front Cell Neurosci* **11**, 279 (2017).
61. R. J. Lucas, Mammalian inner retinal photoreception. *Curr Biol* **23**, R125-133 (2013).
62. R. J. Lucas *et al.*, Identifying the photoreceptive inputs to the mammalian circadian system using transgenic and retinally degenerate mice. *Behav Brain Res* **125**, 97-102 (2001).
63. R. J. Lucas *et al.*, Measuring and using light in the melanopsin age. *Trends Neurosci* **37**, 1-9 (2014).
64. J. W. Maddox, E. Gleason, Nitric oxide promotes GABA release by activating a voltage-independent Ca(2+) influx pathway in retinal amacrine cells. *J Neurophysiol* **117**, 1185-1199 (2017).

65. J. W. Maddox, N. Khorsandi, E. Gleason, TRPC5 is required for the NO-dependent increase in dendritic Ca(2+) and GABA release from chick retinal amacrine cells. *J Neurophysiol* **119**, 262-273 (2018).
66. R. S. Maggesissi *et al.*, Modulation of GABA release by nitric oxide in the chick retina: different effects of nitric oxide depending on the cell population. *Vision Res* **49**, 2494-2502 (2009).
67. R. E. Marc *et al.*, Heterocellular Coupling Between Amacrine Cells and Ganglion Cells. *Front Neural Circuits* **12**, 90 (2018).
68. R. H. Masland, The fundamental plan of the retina. *Nat Neurosci* **4**, 877-886 (2001).
69. R. H. Masland, Neuronal diversity in the retina. *Curr Opin Neurobiol* **11**, 431-436 (2001).
70. R. H. Masland, The neuronal organization of the retina. *Neuron* **76**, 266-280 (2012).
71. S. Maxeiner *et al.*, Deletion of connexin45 in mouse retinal neurons disrupts the rod/cone signaling pathway between AII amacrine and ON cone bipolar cells and leads to impaired visual transmission. *J Neurosci* **25**, 566-576 (2005).
72. A. K. McCauley, W. B. Carden, D. W. Godwin, Brain nitric oxide synthase expression in the developing ferret lateral geniculate nucleus: analysis of time course, localization, and synaptic contacts. *J Comp Neurol* **462**, 342-354 (2003).
73. A. Meyer *et al.*, Connexin30.2: In Vitro Interaction with Connexin36 in HeLa Cells and Expression in AII Amacrine Cells and Intrinsically Photosensitive Ganglion Cells in the Mouse Retina. *Front Mol Neurosci* **9**, 36 (2016).
74. S. L. Mills, S. C. Massey, Differential properties of two gap junctional pathways made by AII amacrine cells. *Nature* **377**, 734-737 (1995).
75. S. L. X. Mills, X; Hoshi, H; Firth, S; Rice, M.E; Frishman, L.J; Marshak, D.W, Dopaminergic modulation of tracer coupling in GC-AC network. *Vis Neurosci* **24**, 593-608 (2007).
76. L. P. Muller *et al.*, Expression and modulation of connexin 30.2, a novel gap junction protein in the mouse retina. *Vis Neurosci* **27**, 91-101 (2010).
77. L. P. Muller, M. T. Do, K. W. Yau, S. He, W. H. Baldridge, Tracer coupling of intrinsically photosensitive retinal ganglion cells to amacrine cells in the mouse retina. *J Comp Neurol* **518**, 4813-4824 (2010).
78. J. O'Brien, H. B. Nguyen, S. L. Mills, Cone photoreceptors in bass retina use two connexins to mediate electrical coupling. *J Neurosci* **24**, 5632-5642 (2004).
79. P. Ostwald, I. M. Goldstein, A. Pachnanda, S. Roth, Effect of nitric oxide synthase inhibition on blood flow after retinal ischemia in cats. *Invest Ophthalmol Vis Sci* **36**, 2396-2403 (1995).
80. F. Pan, D. L. Paul, S. A. Bloomfield, B. Volgyi, Connexin36 is required for gap junctional coupling of most ganglion cell subtypes in the mouse retina. *J Comp Neurol* **518**, 911-927 (2010).
81. J. J. Pang *et al.*, Retinal degeneration 12 (rd12): a new, spontaneously arising mouse model for human Leber congenital amaurosis (LCA). *Mol Vis* **11**, 152-162 (2005).

82. J. J. Pang, F. Gao, S. M. Wu, Light responses and morphology of bNOS-immunoreactive neurons in the mouse retina. *J Comp Neurol* **518**, 2456-2474 (2010).
83. J. J. Pang, D. L. Paul, S. M. Wu, Survey on amacrine cells coupling to retrograde-identified ganglion cells in the mouse retina. *Invest Ophthalmol Vis Sci* **54**, 5151-5162 (2013).
84. L. Perez de Sevilla Muller, S. S. Azar, J. de Los Santos, N. C. Brecha, Prox1 Is a Marker for AII Amacrine Cells in the Mouse Retina. *Front Neuroanat* **11**, 39 (2017).
85. L. Perez De Sevilla Muller, J. Shelley, R. Weiler, Displaced amacrine cells of the mouse retina. *J Comp Neurol* **505**, 177-189 (2007).
86. L. H. Pinto, C. Enroth-Cugell, Tests of the mouse visual system. *Mamm Genome* **11**, 531-536 (2000).
87. V. P. Porciatti, T; Maffei, L., The visual physiology of the wild type mouse determined with pattern VEPs. *Vision Res* **39**, 3071-3081 (1999).
88. G. T. Prusky, N. M. Alam, S. Beekman, R. M. Douglas, Rapid quantification of adult and developing mouse spatial vision using a virtual optomotor system. *Invest Ophthalmol Vis Sci* **45**, 4611-4616 (2004).
89. M. Puopolo, S. E. Hochstetler, S. Gustincich, R. M. Wightman, E. Raviola, Extrasynaptic release of dopamine in a retinal neuron: activity dependence and transmitter modulation. *Neuron* **30**, 211-225 (2001).
90. L. E. Quattrochi *et al.*, The M6 cell: A small-field bistratified photosensitive retinal ganglion cell. *J Comp Neurol* **527**, 297-311 (2019).
91. A. N. Reifler *et al.*, All spiking, sustained ON displaced amacrine cells receive gap-junction input from melanopsin ganglion cells. *Curr Biol* **25**, 2763-2773 (2015).
92. A. N. Reifler *et al.*, The rat retina has five types of ganglion-cell photoreceptors. *Exp Eye Res* **130**, 17-28 (2015).
93. C. Ribelayga, Y. Cao, S. C. Mangel, The circadian clock in the retina controls rod-cone coupling. *Neuron* **59**, 790-801 (2008).
94. V. Riveros-Moreno, C. Beddell, S. Moncada, Nitric oxide synthase. Structural studies using anti-peptide antibodies. *Eur J Biochem* **215**, 801-808 (1993).
95. A. R. Rodriguez, L. P. de Sevilla Muller, N. C. Brecha, The RNA binding protein RBPMS is a selective marker of ganglion cells in the mammalian retina. *J Comp Neurol* **522**, 1411-1443 (2014).
96. K. A. Roecklein *et al.*, Melanopsin, photosensitive ganglion cells, and seasonal affective disorder. *Neurosci Biobehav Rev* **37**, 229-239 (2013).
97. R. Rozental *et al.*, Gap junction-mediated bidirectional signaling between human fetal hippocampal neurons and astrocytes. *Dev Neurosci* **23**, 420-431 (2001).
98. R. Rozental, M. Srinivas, D. C. Spray, How to close a gap junction channel. Efficacies and potencies of uncoupling agents. *Methods Mol Biol* **154**, 447-476 (2001).
99. A. Santos-Carvalho, F. Elvas, A. R. Alvaro, A. F. Ambrosio, C. Cavadas, Neuropeptide Y receptors activation protects rat retinal neural cells against

necrotic and apoptotic cell death induced by glutamate. *Cell Death Dis* **4**, e636 (2013).
100. T. M. Schmidt *et al.*, A role for melanopsin in alpha retinal ganglion cells and contrast detection. *Neuron* **82**, 781-788 (2014).
101. T. M. Schmidt *et al.*, Melanopsin-positive intrinsically photosensitive retinal ganglion cells: from form to function. *J Neurosci* **31**, 16094-16101 (2011).
102. T. M. Schmidt, P. Kofuji, Functional and morphological differences among intrinsically photosensitive retinal ganglion cells. *J Neurosci* **29**, 476-482 (2009).
103. T. M. Schmidt, K. Taniguchi, P. Kofuji, Intrinsic and extrinsic light responses in melanopsin-expressing ganglion cells during mouse development. *J Neurophysiol* **100**, 371-384 (2008).
104. M. M. Schroeder *et al.*, The Roles of Rods, Cones, and Melanopsin in Photoresponses of M4 Intrinsically Photosensitive Retinal Ganglion Cells (ipRGCs) and Optokinetic Visual Behavior. *Front Cell Neurosci* **12**, 203 (2018).
105. T. Schubert *et al.*, Connexin36 mediates gap junctional coupling of alpha-ganglion cells in mouse retina. *J Comp Neurol* **485**, 191-201 (2005).
106. D. Segretain, M. M. Falk, Regulation of connexin biosynthesis, assembly, gap junction formation, and removal. *Biochim Biophys Acta* **1662**, 3-21 (2004).
107. M. L. Semo, D.; Peirson, S.; Butler, J.; Foster, R., Light-induced c-fos in melanopsin retinal ganglion cells of young and aged rodless/coneless (rd/rd cl) mice *Eurpoean Journal of Neuroscience* **18**, 3007-3017 (2003).
108. G. Sohl, K. Willecke, Gap junctions and the connexin protein family. *Cardiovasc Res* **62**, 228-232 (2004).
109. K. B. Sondereker, M. E. Stabio, J. R. Jamil, M. J. Tarchick, J. M. Renna, Where You Cut Matters: A Dissection and Analysis Guide for the Spatial Orientation of the Mouse Retina from Ocular Landmarks. *J Vis Exp*, (2018).
110. G. E. Sosinsky, B. J. Nicholson, Structural organization of gap junction channels. *Biochim Biophys Acta* **1711**, 99-125 (2005).
111. B. K. Stafford, M. B. Manookin, J. H. Singer, J. B. Demb, NMDA and AMPA receptors contribute similarly to temporal processing in mammalian retinal ganglion cells. *J Physiol* **592**, 4877-4889 (2014).
112. H. G. Taschenberger, R., Several types of Calcium channels mediate glutamatergic synaptic responses to activation of single Thy-1-Immunolabeled Rat Retinal Ganglion Cells. *Journal of Neuroscience* **15**, 2240-2254 (1995).
113. W. B. W. Thoreson, P., Glutamate receptors and circuits in the vertebrate retina. *Progress in Retinal and Eye Reseach* **18**, 765-810 (1999).
114. J. Z. Tsien, P. T. Huerta, S. Tonegawa, The essential role of hippocampal CA1 NMDA receptor-dependent synaptic plasticity in spatial memory. *Cell* **87**, 1327-1338 (1996).
115. J. Turecek *et al.*, NMDA receptor activation strengthens weak electrical coupling in mammalian brain. *Neuron* **81**, 1375-1388 (2014).
116. F. J. Valiente-Soriano *et al.*, Distribution of melanopsin positive neurons in pigmented and albino mice: evidence for melanopsin interneurons in the mouse retina. *Front Neuroanat* **8**, 131 (2014).

117. R. W. M. P. S. H. D. I. Vaney, Modulation of coupling between retinal horizontal cells by retinoic acid and endogenous dopamine. (2000).
118. G. Vartanian, K. Y. Wong, P. C. Ku, LED Lights With Hidden Intensity-Modulated Blue Channels Aiming for Enhanced Subconscious Visual Responses. *IEEE Photonics J* **9**, (2017).
119. A. H. Vielma, A. Agurto, J. Valdes, A. G. Palacios, O. Schmachtenberg, Nitric oxide modulates the temporal properties of the glutamate response in type 4 OFF bipolar cells. *PLoS One* **9**, e114330 (2014).
120. T. J. Viney *et al.*, Local Retinal Circuits of Melanopsin-Containing Ganglion Cells Identified by Transsynaptic Viral Tracing. *Current Biology* **17**, 981-988 (2007).
121. B. Volgyi, J. Abrams, D. L. Paul, S. A. Bloomfield, Morphology and tracer coupling pattern of alpha ganglion cells in the mouse retina. *J Comp Neurol* **492**, 66-77 (2005).
122. B. Volgyi, T. Kovacs-Oller, T. Atlasz, M. Wilhelm, R. Gabriel, Gap junctional coupling in the vertebrate retina: variations on one theme? *Prog Retin Eye Res* **34**, 1-18 (2013).
123. O. J. Walch *et al.*, Characterizing and modeling the intrinsic light response of rat ganglion-cell photoreceptors. *J Neurophysiol* **114**, 2955-2966 (2015).
124. P. Witkovsky, Dopamine and retinal function. *Doc Ophthalmol* **108**, 17-40 (2004).
125. X. B. Xia, S. L. Mills, Gap junctional regulatory mechanisms in the AII amacrine cell of the rabbit retina. *Vis Neurosci* **21**, 791-805 (2004).
126. D. Xin, S. A. Bloomfield, Tracer coupling pattern of amacrine and ganglion cells in the rabbit retina. *J Comp Neurol* **383**, 512-528 (1997).
127. L. Xinbo *et al.*, Connexin45-Containing Neuronal Gap Junctions in Rodent Retina Also Contain Connexin36 in Both Apposing Hemiplaques, Forming Bihomotypic Gap Junctions, with scaffolding Contributed by Zonula Occludens-1. *The Journal of Neuroscience* **28**, 9769-9789 (2008).
128. D. Yu, W. D. Eldred, Gycine and GABA interact to regulate the nitric oxide/cGMP signaling pathway in the turtle retina. *Vis Neurosci* **22**, 825-838 (2005).
129. D. Q. Zhang *et al.*, Intraretinal signaling by ganglion cell photoreceptors to dopaminergic amacrine neurons. *Proc Natl Acad Sci U S A* **105**, 14181-14186 (2008).
130. X. Zhao, B. K. Stafford, A. L. Godin, W. M. King, K. Y. Wong, Photoresponse diversity among the five types of intrinsically photosensitive retinal ganglion cells. *J Physiol* **592**, 1619-1636 (2014).
131. C. Zhou, R. F. Dacheux, All amacrine cells in the rabbit retina possess AMPA-, NMDA-, GABA-, and glycine-activated currents. *Vis Neurosci* **21**, 181-188 (2004).
132. L. Zhou, D. Y. Zhu, Neuronal nitric oxide synthase: structure, subcellular localization, regulation, and clinical implications. *Nitric Oxide* **20**, 223-230 (2009).